12-2020

Development of a Single Emitter Ionic Liquid Ion Source Research Platform

Thomas V. Kerber
Western Michigan University, thomaskerber689@gmail.com

DEVELOPMENT OF A SINGLE EMITTER IONIC LIQUID ION SOURCE RESEARCH PLATFORM

by

Thomas V. Kerber

A thesis submitted to the Graduate College
in partial fulfillment of the requirements
for the degree of Master of Science
Mechanical and Aerospace Engineering
Western Michigan University
December 2020

Thesis Committee:

Kristina Lemmer, Ph.D., Chair
Nicholas Taylor, Ph.D.
Tianshu Liu, Ph.D.

DEVELOPMENT OF A SINGLE EMITTER IONIC LIQUID ION SOURCE RESEARCH PLATFORM

Thomas V. Kerber, M.S.

Western Michigan University, 2020

A single emitter ionic liquid ion source using porous borosilicate glass was developed. Two emitters with different radii of curvatures were tested using 1-ethyl-3-methylimidazolium tetrafluoroborate (EMI-BF_4). I-V curves of the currents on the extractor electrode and a collector plate were obtained for potential differences between the emitter and the extractor ranging from 0 V to 3500 V. For the first emitter chip, extraction began near 2400 V. The highest emission current measured on the first chip was 80 μA at 3500 V with an interception current on the extractor of 4.86 μA. An new collector plate was used to obtain I-V traces of the second emitter chip for potential differences between the emitter and the extractor ranging from 0 V to 3300 V. The second emitter had a sharper tip and emission began between 2000 V and 2200 V on the emitter. The highest emission current of 50 μA using the second chip was at the peak applied voltage of 3300 V with a corresponding interception current of 0.71 μA. An electron suppression grid on the collector plate was tested to minimize the effect of secondary electron emission from the surroundings. Results show a substantial increase in collector current when a negative bias is applied to the grid implicating that electrons from secondary electron emission were successfully rejected.

ACKNOWLEDGMENTS

First I must acknowledge and thank my advisor, Dr. Kristina Lemmer, for all the technical, professional, and academic support you have provided during my time at ALPE. I would also like to thank Dr. Nicholas Taylor for the initial push to start ALPE on researching electrosprays thereby instigating the work in this thesis and for the technical guidance you've provided throughout it. I'd like to thank all the current and past ALPE members I've worked with including: Margaret Mooney, Hannah Watts, Ron McGee-Sinclair, Nagual Simmons, and Dr. Matthew Baird. With you all there the research at the lab is not just an interesting challenge but also exciting and fun. Lastly, I'd like to thank my friends and family for their support and infinite patience during my long winded and confusing explanations whenever you asked about what I was working on.

Thomas V. Kerber

TABLE OF CONTENTS

Table of Contents–Continued

LIST OF FIGURES

List of Figures–Continued

CHAPTER 1

INTRODUCTION

Small satellites (sub 500-kg) are the fastest growing form of scientific and commercial space mission [1]. Nanosatellites, microsatellites, and Cubesats are all classes of small satellites which have rapidly transitioned from a purely educational tool to commercial and scientific applications due to their lower cost, shorter development times, and frequent launch opportunities. Each of these factors enable smaller organizations, like universities and start-ups, to perform new science and develop new technology at reasonable costs. These benefits are also being leveraged by larger companies, NASA, and the military to enable more specialized activities at lower cost, such as SpaceX's StarLink, and Iridium, two low Earth orbit (LEO) communication satellite constellations [2]. Without efficient propulsion, small satellites have limited capabilities from a lack of spatial control and transport. Most small satellite missions are carried out in LEO which imposes certain constraints on a spacecraft without active propulsion. For extended missions in LEO, atmospheric drag must be considered and North-South station-keeping is often necessary. For many LEO orbits, propulsion must be used for de-orbit at end of life [3]. Additionally, precision pointing and orbit raising are required to achieve objectives for many applications [4]. Chemical propulsion systems are typically not a viable option due to propellant tank size requirements and risk to the parent spacecraft from pressurized and combustible propellants. Cold-gas systems have been used, but are bulky and provide very limited and short-term propulsion. Most electric propulsion (EP) systems, such as Hall effect thrusters and ion engines, have not been efficiently scaled down to sizes compatible with traditional 3U and 6U cubesats [5]. Therefore, a growing focus is being placed on developing micropropulsion technologies that provide higher performance at lower cost, volume, and mass.

There are many different technologies that fall under the electric propulsion umbrella some of which scale to low power more readily than others. EP is divided into three main categories

based on the mechanism used to create thrust: electrostatic, electromagnetic, and electrothermal. Electrostatic thrusters use fixed electric fields to accelerate ions, common thrusters of this type are ion engines, Hall effect thrusters, and electrospray thrusters. Electromagnetic thrusters, such as magnetoplasmadynamic thrusters and pulsed plasma thrusters, use Lorentz forces or other electromagnetic effects to accelerate the propellant. Electrothermal devices, such as arcjets and resistojets, use electricity to heat the propellant expanding it through a nozzle, generally providing better I_{sp} compared with cold gas or chemical nozzle thrusters. Each of these devices converts electrical energy into thrust without utilizing energy stored in chemical bonds making them electric propulsion devices [6].

1.1 Electric Propulsion and Small Satellites

Thrust, total efficiency, and specific impulse are the primary performance metrics for a propulsion system when mission planning. Total efficiency is the product of several experimentally determined efficiencies of the system. The final result is the beam power normal to the thruster divided by the total input electrical power. Specific impulse (I_{sp}) is the change in momentum a propulsion system delivers per kg of propellant. [6]. Mathematically, it is the ratio of the propellant exhaust velocity to the standard gravitational acceleration of Earth, g. The impact of I_{sp} on spacecraft performance is best shown using the ubiquitous rocket equation given in Eq. 1.1. Increasing the specific impulse will either increase the total available change in velocity (ΔV) of the spacecraft or decrease the propellant to delivered mass ratio, m_p/m_d, for a set ΔV.

$$\frac{m_p}{m_d} = exp\left(\frac{\Delta V}{gI_{sp}}\right) - 1 \tag{1.1}$$

While thrust, efficiency, and specific impulse must be considered when selecting a propulsion system; there are challenges unique to small satellite missions that must be addressed. First, the system must require very little power to operate. Small satellites, especially < 100 kg, are power constrained; capable of providing only 10-1000 Watts. Second, the propulsion system must be compact and require minimal propellant. Without careful design, propellant storage and the thruster head can encroach on volume and weight required for payload. Furthermore, propulsion systems that require pressurized propellants like Hall effect, gridded ion, cold-gas, and chemical

thrusters require additional mass for the storage tank and flow control system to prevent failures. This makes thrusters with liquid or solid propellants attractive options as vehicles are miniaturized. Third, subsystem components sensitive to EM noise do not have the space to be isolated from thrusters that emit radiation. Therefore, an ideal propulsion system will generate low levels of EM noise [7].

Four types of EP that have been used on smallsat missions to date and satisfy the requirements discussed best are the pulsed plasma thruster (PPT), vacuum arc thruster (VAT), micro gridded ion engine, and electrospray thruster. The PPT and VAT are similar pulsed power devices that evaporate a solid or sometimes liquid propellant with a high-voltage pulse. The ablated material is accelerated by a JxB Lorentz force in the case of a PPT, and by a magnetic pressure gradient for the VAT. PPTs and VATs provide I_{sp} in the mid-1000 s range with efficiencies below 20% [8]. Micro gridded ion engines operate by accelerating a plasma through a positive and negative biased grid. These devices are more complex than other types of micro electric propulsion, as they require a plasma source as well as a cathode for neutralization. Plasma can be generated either using RF power or an additional cathode for electron-ion bombardment. This necessitates multiple power supplies along with the higher complexity required by a gas propellant feed system. Micro gridded ion engines have the benefit of higher I_{sp} in the 2000 s range but suffer from very low total efficiency below 30% [9]. Finally, electrospray thrusters are one of the most promising emerging technologies to fill this micropropulsion technology void. Several electrospray thrusters in development project efficiencies of 60-80% and specific impulses up to 1,500 s.

1.2 Motivation and Scope of Research

The usefulness of electrospray technology extends far beyond nano/microsatellites and even beyond propulsion. Historically, the primary scientific application for electrosprays is as a soft ionization technique for mass spectrometry of large organic molecules [10]. The benefits of electrosprays, namely very precise thrust increments with low thrust noise, lend themselves perfectly for precision pointing, formation flying, and drag compensation. An excellent example is the Laser Interferometer Space Antenna (LISA). This mission involves detecting gravitational waves by measuring picometer length changes between three spacecraft separated by 2.5 million

kilometers. A colloid electrospray thruster developed by Busek was used on the LISA Pathfinder mission and will enable the LISA mission by creating a virtually drag-free environment so any fluctuation in distance between the spacecraft can be detected [11]. Another mission enabled by the unique capabilities of electrospray thrusters is HabEx, a proposed exoplanet observatory requiring precision pointing between a telescope and a 52-m-diameter starshade that is located 76 km away [12].

Electrospray thrusters occupy a unique domain in the micro-propulsion field with their high I_{sp}, low temperature operation, liquid propellant, and flexible power scaling. These attributes position them well to fill the technology gap between the expanding desire for propulsion on shrinking satellites and state-of-the-art thruster technology. Western Michigan University's (WMU) Aerospace Laboratory for Plasma Experiments (ALPE) is continually seeking new avenues for researching space propulsion technologies. The relatively simplistic design of an electrospray thruster along with their low mass flow-rates make them ideally suited for study at ALPE. The increasing demand for micropropulsion systems on small satellites adds drive to this research via relevance to the interests of every sector of space.

The development of a modular electrospray has expanded ALPE's research capabilities into an new domain of electric propulsion research and will continue to enable new experimental campaigns. To date, operation of electrosprays in-space has been limited to technology demonstration missions. Reliability issues driven by a limited understanding of operating principles have constrained the technology's usability [13] [14]. Before electrosprays are an enabling technology significant research efforts must overcome their limited lifetimes and address several efficiency deficits. The work completed in this thesis lays the foundation for ALPE's participation in this process.

This thesis encompasses the design, building, and initial operational validation of a single emitter laboratory electrospray test cell. This thruster does not seek to be flight-like or even necessarily have a path towards flight hardware. The primary goal of this thruster is to be a laboratory platform to enable experimental campaigns investigating fundamental operating principles of electrosprays at WMU. The thesis will also include several suggested paths forward to continue electrospray research at WMU that are relevant to the field of electric propulsion. Diagnostics of the developed electrospray thruster are limited to operation telemetry as full characterization of

the beam is outside the scope of this thesis. The design is simple with a focus on allowing easy modifications for future studies.

1.3 Thesis Composition

This thesis is divided into 5 chapters. Chapter 1 provides context and motivation for the development of a research electrospray thruster at ALPE. Chapter 2 covers the theory of operation, typical geometry layout, and common methods for experimentally investigating operation of an electrospray along with a brief history of their development and use as a propulsive device. Chapter 3 presents the designs of the first thruster made for this thesis along with the experimental setup and testing procedures. Chapter 4 presents data from several tests of the thruster using different experimental setups and emitter chips and discusses their implications. Chapter 5 summaries the results of the development process and the results from preliminary experiments. This chapter also includes a discussion of updates to the thruster based on the results that will enable future research.

CHAPTER 2

BACKGROUND

2.1 History of Electrospray Devices

The effect of electrostatic fields on a liquid has been known since the early days of electricity research using amber. Observation of a cone forming in the presence of a sufficiently intense electric field dates back to 1600 by William Gilbert. Investigation of this phenomenon continued as new methods for generating a discharge were discovered; however, few practical applications were devised. Different spraying regimes were visually characterized as a function of discharge voltage and emitter geometry but the research did not grow past observation and discussion. A significant milestone in the field was Sir Geoffrey Taylor's calculations of the required electric field to form a cone and of that cone's half angle, 49.3° [15]. Starting with this work a more in depth analysis of the phenomenon began, and several groups began developing uses for the electrospray process. Arguably, the most significant role electrosprays have played is in organic chemistry as a highly efficient method for forming large molecular ions. This is an extremely powerful tool for mass spectrometry where proteins are ionized for identification without significant fragmentation. John Fenn eventually received a Nobel Prize in chemistry for his role in the development of this technique. Capillary based electrosprays have been consistently utilized in mass spectrometry, and there have been many innovations since their initial development. This has lead to a number of important applications such as the rapid and accurate identification of protein molecules and the study of noncovalent complexes in molecules [16].

Electrosprays have proven valuable in a number of other fields including: conventional and nano-manufacturing [17], gas-phase chemistry, and space propulsion. Soon after Taylor's experiments, the colloid thruster was theorised as a potential propulsive device. A thruster using a glycerol solution doped with NaI as propellant was developed for a demonstration mission on a

geosynchronous satellite [18]. However, due to the severally limited amount of thrust and required bias potential reaching into the 10's of kV, interest in colloid thrusters waned, and the mission was never flown. The advent of smallsats in the 90's along with advances in Micro-Electro-Mechanical Systems (MEMS) manufacturing techniques rekindled interest in electrosprays as propulsive devices. Additionally, the use of highly conductive ionic liquids reduced the necessary discharge voltage, further enabling the technology [19]. A number of thruster concepts were designed and tested over the next two decades but a true colloid thruster was not used for propulsion in space until 2015 on the LISA Pathfinder mission. The Colloid MicroNewton Thrusters (CMNTs), developed by Busek Co. Inc. developed for the mission operated in space for over 2,400 hours and provided micronewton thrust achieving all of the demonstration missions objectives [20]. Since then, seven other spacecraft have used electrospray propulsion, all of which have been technology demonstration missions. Three organizations have developed the thrusters with flight heritage, Busek made the CMNTs for the LISA pathfinder mission. Researchers at MIT designed the thrusters for the Aerospace Corporation's AeroCube satellites. That technology was further developed by MIT's spinoff company Accion Systems, who built the electrosprays for the Irvine Cubesats. Enpulsion, based out of Vienna, Austria, has developed and flown the Enpulsion Nano, a 10 W field emission electric propulsion (FEEP) thruster [21].

Research into electrospray thruster technology has exploded over the last 20 years. Potential as a micropropulsion device for smallsats and as high fidelity drag compensation for creating virtual drag-free environments has driven a large number of organizations to pursue electrospray research. MIT is developing the Scaleable ion Electrospray Propulsion system (S-iEPS) a porous emitter based electrospray that uses ionic liquids to achieve $74\mu N$ of thrust at > 1150 s specific impulse [22]. The Air Force Research Laboratory (AFRL) is developing the Air Force Electrospray Thruster (AFET). AFET is a fully conventionally machined electrospray utilizing a porous glass emitter which has produced $40\mu N$ of thrust [23]. A number of groups are also conducting electrospray experiments on laboratory thrusters to better understand the fundamental physics including, UCLA, USC, MIT, University of California, Irvine, and NASA Glenn Research Center (GRC) [20] [24] [25] [26]. These are in addition to the companies listed previously who have flown electrosprays and an increasing number of companies developing their own thrusters.

As propulsive devices three main challenges need to be addressed before widespread adop-

tion is possible. First, several mechanisms drive a shorter operational lifetime than required when proposed missions necessitate 1,000's of hours of thrust. Chemical decomposition of the propellant, emitter tip erosion, and emitter-extractor grid shorting from ion impingement on the extractor are the three main processes that lead to shorter lifetimes. Validating lifetime models with experimental data is a major area of research working to address these mechanisms [20]. The second challenge is lower than theorised efficiency. Several factors contribute to efficiency losses including: beam divergence, molecular composition of the plume, and ion interception on the extractor grid. Finally, for any electric propulsion device effective neutralization of the beam is critical otherwise free ions will eventually return to the spacecraft in a potentially destructive manner. For many plasma based thrusters this is done with a hollow cathode that emits electrons next to the discharge beam. While this is technically an option for an electrospray, the addition of a cathode would significantly increase system complexity, reduce total efficiency, and introduce failure mechanisms. Furthermore, it is not always viable in micro or nanosatellite applications. Neutralization of the beam by either polarity switching of a single thruster or parallel operation of two opposite polarity thrusters has been theorised and tested by several groups [27]. However, it has not been studied in a sufficiently rigorous manner to assure its effectiveness in-space.

2.2 Types of Electrosprays

Electrosprays eject propellant in two different modes. Colloid thrusters operate in a droplet regime where discrete large clusters of propellant are ejected from the needle in regular intervals. Colloid thrusters operate at the highest thrust but with the lowest efficiency and I_{sp} compared to other electrospray designs due to larger mass flow rates at lower exhaust velocities [11]. At the apex of a colloid thruster the propellant typically forms a cone-jet that eventually breaks up into droplets. The second mode is called the pure ionic regime (PIR), where only single ions or clusters of two or three molecules are emitted. Single ions can be accelerated more quickly resulting in higher I_{sp} but lower thrust. In PIR, efficiency is affected by the plumes composition. Single ions (monomers) are more efficient to accelerate compared to a cluster of one whole molecule and an ion (dimer) or two molecules and an ion (trimer). It is possible for a thruster to operate in either mode with the necessary flow rate and discharge voltages. However, performance will suffer if the

thruster is not designed for that mode.

Electrospray thrusters can be categorized by their propellant focusing system. The three common methods are; capillary needles, porous emitters, and externally-wetted emitters. The propellant is delivered either passively by capillary forces in the case of porous and externally-wetted emitters or is controlled by liquid pumps for capillary needles. In all cases thrusters can be composed of a single emitter or an array of emitters with varying packing densities to control total thrust. Electrosprays for mass spectrometry and other non-propulsion applications are most often capillary emitters. Direct control over flow rates, ease of manufacturing, and simple assemblies make them ideal for these applications. Capillary needles are also used for colloid type electrospray thrusters. The CMNTs on the LISA pathfinder mission are an example of colloid thrusters which highlights their benefit of having longer operational times than current designs for passively fed electrospray thrusters. Capillary electrosprays are also beneficial for laboratory experiments for their relative ease of design and setup and are commonly used for studying the fundamental physics of electrospray operation. Externally-wetted emitters are most commonly seen in Field Emission Electric Propulsion (FEEP) devices which use liquid metal propellants like indium and cesium. A group from MIT has also designed an externally-wetted electrospray using the ionic liquid $EMI-BF_4$ [28]. FEEP thrusters are a subset of electrosprays and also lack significant flight heritage. They typically provide much lower thrust than ionic liquid electrosprays, between $1\mu N$ and 1 mN, at a higher I_{sp}, between 6,000-12,000 s.

Recently, the significant research and development focus has been placed on porous emitters, as their performance regime is more relevant to the current smallsat driven boom in micropropulsion. Porous emitters are known for operating at low flow rates compared to capillary electrosprays. This enables them to operate in the purely-ionic regime (PIR). Metal foam, typically tungsten, but nickel alloys have also been tested, was first used for porous emitters due to the available manufacturing methods [29]. However, metallic foams suffer from several performance and manufacturing challenges. Metallic foams have a strong tendency to erode over time from electrochemical etching by the ionic liquid. This can be mitigated by alternating the extractor polarity at a frequency near 1 Hz which maintains a balance between the cation and anion, limiting chemical degradation. Furthermore, the electrochemical etching process used to manufacture tungsten emitters can be inconsistent and requires significant investment in specialized equipment. As a result,

dielectric materials, specifically fritted borosilicate, are being investigated as an alternative emitter substrate. Borosilicate glass is resistant to chemical degradation and can be manufactured using conventional methods, making it ideal for eletrospray emitters [25]. Dielectric emitters do require an additional component called a distal grid which is an electrode placed in contact with the ionic liquid to provide a current path to for propellant [30].

2.3 Principles of Operation

Electrosprays operate via a high potential difference between a field enhancing structure and a downstream electrode that extracts and accelerates ions or droplets from a conductive liquid. The electric field is generated by either grounding the extracting electrode and biasing the emitter or the reverse. An additional accelerator electrode can be included downstream of the extractor to increase exhaust velocity and prevent electrons from back streaming into the emitters. Ion emission occurs by the formation of a Taylor cone created by electric field enhancement on the order of 1 V/nm at the emitter tip. The Taylor cone further amplifies the electric field until the fluid becomes unstable forcing ions to be emitted at the tip [22]. This emission occurs for several different modes and levels of stability. Single droplets or ions, a steady cone-jet or an unsteady cone-jet can all be emitted, depending on the liquid used, electrospray geometry, mass flow rate, and discharge potential. These modes affect performance with cone-jet and droplet modes having higher thrust and lower specific impulse compared to the purely ionic regime's (PIR) high specific impulse and low thrust. Fig 2.1 shows a simplified schematic of a porous-type electrospray with an accelerator grid and the electrical circuit for the extractor and emitter.

Porous-media based electrosprays typically use a room temperature molten salt, called an ionic liquid, which is stored in a porous glass reservoir below the emitter. These types of thrusters are referred to as ionic liquid ion sources (ILIS) and are more likely to operate in PIR than capillary needle electrosprays. Ionic liquids have negligible vapor pressure along with a viscosity that enables effective capillary action within porous media making them ideally suited for space propulsion. 1-ethyl-3-methylimidazolium tetrafluoroborate ($EMI-BF_4$) and bis(rifluoromethylsulfonyl)imide ($EMI-Im$) are highly-conductive ionic liquids and the most common propellants for porous electrosprays [26]. The larger pores of the reservoir create a Laplace pressure driving the propellant

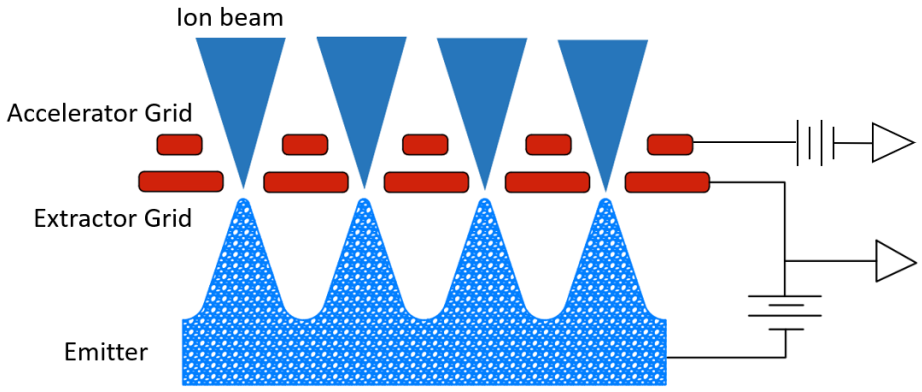

Figure 2.1: Diagram of a porous-media based electrospray with accelerator grid.

to the emitter without the need for an active feed system [31]. The emitted ions are then accelerated through an orifice in the extractor electrode creating the beam. An ILIS only accelerates the cation or the anion of the propellant at one time depending on the discharge bias. This imbalance is a primary mechanism in several of the previously mentioned challenges for electrosprays. If large quantities of only one ion are removed, the propellant will become chemically imbalanced, affecting fluid properties and reducing efficiency and specific impulse. Damaging electrochemical reactions occurs when the potential difference across the electrode-fluid interface called the double layer exceeds the ionic liquids electrochemical window limit. Additionally, this propellant degradation can contribute to etching on emitters, further reducing performance and eventually resulting in failure. Imbalanced charge emission is also fundamentally the driver for requiring beam neutralization. Polarity switching at $>$1 Hz as well as careful selection of where to electrically connect to the propellant increases how long saturation of the electrochemical double layer takes but requires a slightly more complex design and power processing unit [30].

Electrosprays can be further subdivided into experimental or flight-driven design, depending on their intended application. Flight thruster design focuses heavily on performance, lifetime, and reliability in addition to the requirements for use in smallsats laid out in chapter 1. Depending on the targeted user, flight-driven thrusters strive for higher thrust densities with arrays of tightly packed emitters or for precision attitude control and drag-compensation with fewer emitters. Sizing the propellant reservoir must be done to provide sufficient propellant over the lifetime of the thruster, which can be 1000's of hours. Conversely, experimental laboratory electrospray thruster

design requirements can be more relaxed. Typically, the design is focused on ease of use, modularity, and diagnostic access to the emitters. Emitter density is usually scaled down, and single emitters are often used to decrease variables within the system [32]. Laboratory designs can also include specialized geometries or materials for testing new emitter or extractor layouts. Electrospray test cells cost significantly less than flight designs due to more material options and more flexible tolerances.

Electrospray performance can be characterized in a manner similar to other electric propulsion devices with thrust, specific impulse (I_{sp}), and total efficiency (η). Thrust can be calculated using Eq. 2.1 if the exhaust velocity, v_e, and propellant mass flow rate, $\dot{m}$, are known. However, it is more commonly obtained directly using a thrust stand, eliminating several measurement uncertainties encountered when calculating it indirectly.

$$T = \dot{m} v_e \tag{2.1}$$

The exhaust velocity can be calculated using Eq. 2.2 assuming the charge to mass ratio (q/m) of the emitted particles is known.

$$v_e = \sqrt{\frac{2q\phi}{m}} \tag{2.2}$$

where ϕ is the applied potential between the emitter and extractor. Considering Eq. 2.1 and Eq. 2.2, for passively-fed ILISs thrust per emitter can only be increased by increasing exhaust velocity which requires increasing discharge voltage. The extent to which discharge voltage can be increased is constrained by space-charge limitations between the emitter tip and extractor grid in addition to short characteristic lengths susceptible to electrical shorting.

Efficiency, given in Eq. 2.3, is a product of the experimentally determined polydispersity (η_p), transmission (η_{tr}), energy (η_e), ionization (η_i), and beam divergence (η_{div}) efficiencies.

$$\eta = \eta_p \eta_{tr}^2 \eta_e \eta_i \eta_{div} \tag{2.3}$$

Polydispersity efficiency is unique to electrosprays and accounts for the fact that the beam consists of monomers, dimers, and trimers. Transmission efficiency is the ratio of the beam current, I_b, to the emission current, I_{em}, as shown in Eq. 2.4.

$$\eta_{tr} = \frac{I_b}{I_{em}} \tag{2.4}$$

where I_b is the difference between the emission current and the current drawn on the extractor grid. Emission current is measured using a beam dump in front of the thruster. Beam divergence efficiency is particularly relevant to electrosprays as it represents one of the most significant efficiency losses for the thruster. Beam divergence is calculated by measuring the angular distribution of ion current densities in the exhaust plume and integrating a normalized probability distribution function of these data. The efficiency of the integrated normalized angular ion current distribution (θ_{eff}) is calculated using Eq. 2.5.

$$\eta_{div} = cos^2(\theta_{eff}) \tag{2.5}$$

The potential required to deform the ionic liquid into a Taylor cone and begin emission can be estimated using Eq. 2.6 derived from balancing the hydrodynamic forces with the electrostatic forces.

$$V_{start} = \sqrt{\frac{\gamma R_c}{\varepsilon_0}} \ln\left(\frac{4d}{R_c}\right) \tag{2.6}$$

where γ is the surface tension, R_c is the radius of curvature of the emitter, ε_0 is the permittivity of free space and d is the distance of the emitter from the extractor. This equation is formulated using several assumptions for the emitter and extractor geometry as well as emission physics [33]; however, it remains a useful tool for estimating the necessary voltage with only a select number of parameters for a given electrospray device. Eq 2.7 describes the same phenomenon but is derived using different assumptions and results in a factor of 1/2 in the natural log term [34]. From the results, both estimates under represent the starting voltage with Eq. 2.6 being slightly more accurate.

$$V_{start} = \sqrt{\frac{\gamma R_c}{\varepsilon_0}} \ln\left(\frac{4d}{2R_c}\right) \tag{2.7}$$

Due to the high voltage and small geometry in electrospary devices, it is important to consider the Paschen breakdown voltage so that arcing does not occur and damage the system.

This breakdown voltage can be calculated using Eq. 2.8.

$$V_B = \frac{Bpd}{Ln(Apd) - ln[ln(1+\frac{1}{\lambda_{se}})]} \tag{2.8}$$

where p (Pa) is the pressure, d (m) is the gap distance, λ_{se} is the secondary electron emission (SEE) coefficient, A is ionization saturation as a function of electric field/pressure, and B is a function of excitation and ionization energies. It is difficult to determine an exact breakdown voltage using Paschen's curve because the measured pressure of the chamber is not the same as the local pressure at the electrospray emitter tip. Additionally, Paschen's curve relies on several assumptions of ion and electron formation that make it more useful as a guideline for design than a true analysis of the system.

2.4 Operational Characterization

The first component of characterizing electrospray thrusters is examining operating telemetry such as discharge voltage, beam current, and extractor grid intercepted current. By mapping discharge voltage to these currents, nominal operating set points can be determined. Obtaining thrust directly or indirectly is another important step, especially for flight thrusters, and can be used in conjunction with I-V curves to calculate efficiency and find optimal operation conditions. Beam current is usually measured by placing an electrode downstream of the thruster and measuring the resulting current on the plate. Thrust can be estimated if the charge to mass ratio of the beam is known. It can be measured directly using highly sensitive balances or a torsional thrust stand. In addition to operational telemetry, beam composition is vital to understanding operation and requires several different diagnostic tools to fully characterize.

For any electric propulsion testing campaign there are a standard pool of diagnostic tools used to characterize the thruster plume. These include Faraday probes, Langmuir probes, and Retarding Potential Analysers (RPAs). For electrosprays, mass spectrometry is another vital tool for assessing performance because the charge to mass ratio of emitted particles plays a vital role in characterizing thruster operation. Time of flight (ToF) spectrometers are the standard method for obtaining charge to mass ratios for electrospray thrusters. They are typically composed of a gate assembly, the flight tube, and a collector as shown in Figure 2.2. By closing an electrostatic gate

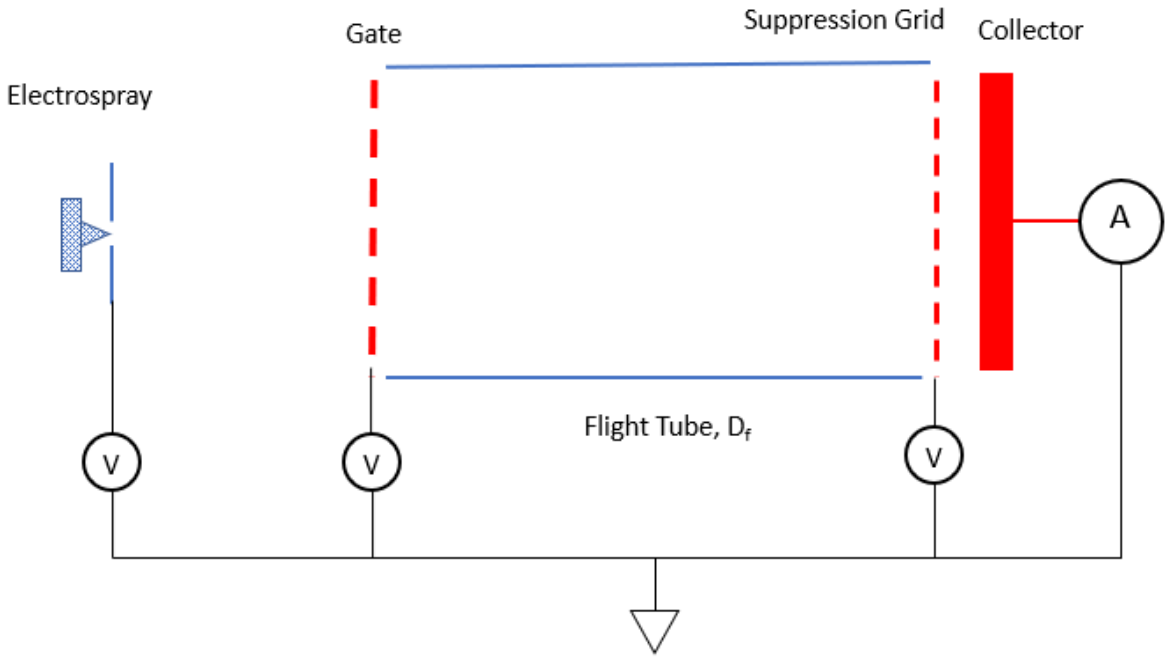

Figure 2.2: Schematic of time-of-flight spectrometer.

that repels emitted ions and measuring the current decay time, t, on an electrode that is a distance D_f downstream of the gate, the mass of the ion can be estimated using Eq. 2.9.

$$m(t) = 2qV_b \left(\frac{t}{D_f}\right)^2 \tag{2.9}$$

where V_b is the beam voltage and q is the elementary charge. The collected current is plotted against the calculated $m(t)$ and the discrete decreases in current correspond with the monomers, dimers, and trimers [23].

A scanning Faraday probe consists of a flat single-sided disk with a biased guard ring. The disk and guard ring are both negatively biased to reject electrons and collect ions from the plasma beam. This is used to determine the beam profile, ion current density, and integrated beam current. This measurement also provides data to determine the beam divergence half-angle, which is the angle of the beam that includes 95% of the momentum-weight ion current [35].

A Langmuir probe is one of the simplest but most useful plasma diagnostic tools. The basic version of a Langmuir probe an electrode biased with an applied voltage sweep. Measurements of the plasma-induced current at an applied potential are used to create a current-voltage trace which is analyzed to determine characteristics of the plasma, including local plasma potential, electron

temperature, electron density, and ion density. Langmuir probes can be mounted to motion tables so that they can be sweep around the thruster to determine how these beam characteristics change around the thruster [36].

RPAs consist of four grids. An attenuation grid in front, a negatively biased electron repelling grid, a retarding grid that is swept over a range of positive voltages, and a second negatively biased grid suppression to reduce signal error from SEE at the collector surface. Measurements from an RPA consist of the ion current on the collecting surface as a function of retarding grid bias potential. The collected current is proportional to the number of ions per unit charge that have sufficient energy to pass the positively biased grid. RPAs are used to measure the plume divergence half angle along with the ion energy distribution function (IEDF) of the beam which is an indicator of the acceleration efficiency of the thruster [37].

CHAPTER 3

THRUSTER DESIGN AND EXPERIMENTAL SETUP

3.1 Thruster Design

The first thruster designed for this thesis is a simplified model that was used as proof-of-concept for design principles of future laboratory thrusters. It acts as a platform for developing operating procedures and a baseline for potential single emitter electrospray experimental campaigns. The Western Single Emitter Laboratory Electrospray (WeSELE) is based around a 1 mm-tall P5 (pore size of 1.0-1.6 μm) porosity borosilicate emitter. In this thesis two emitter chips were fabricated and tested, emitter chip 1 (EC1) with a radius of curvature $\approx$0.1 mm, and emitter chip 2 (EC2) with $\approx$0.03 mm. The emitter is stacked on top of a piece of filter paper for improved fluid connection with a 10 mm-diameter P4 (pore size of 10-16 μm) borosilicate disc which acts as a propellant reservoir. These pore sizes were selected based on a study by Courtney *et. al* [31] which compared various reservoir porosities and showed that using the P4 in conjunction with the P5 grade produced the most ionic beam when using EMI-BF_4.

This stack is housed inside a polyether ether ketone (PEEK) base, and hydraulic contact between the components is insured by tightening a rigid stainless steel plate that also acts as the distal electrode. The last component is the 0.051 mm thick molybdenum extractor plate with a 1.85 mm diameter orifice positioned above the emitter using two ceramic washers. Figure 3.1 shows a cross-sectioned model of the electrospray single emitter along with the finished assembly.

EMI-BF_4 was selected as the propellant because of its ubiquity in ILIS thrusters, allowing for more direct comparison between the laboratory thruster and experiments from the electrospray community. Additionally, there is a large collection of published research on the properties and performance of EMI-BF_4 as a propellant. A single emitter was selected for several reasons. First, it simplifies the manufacturing process of both the emitter and the extractor grid, enabling precise

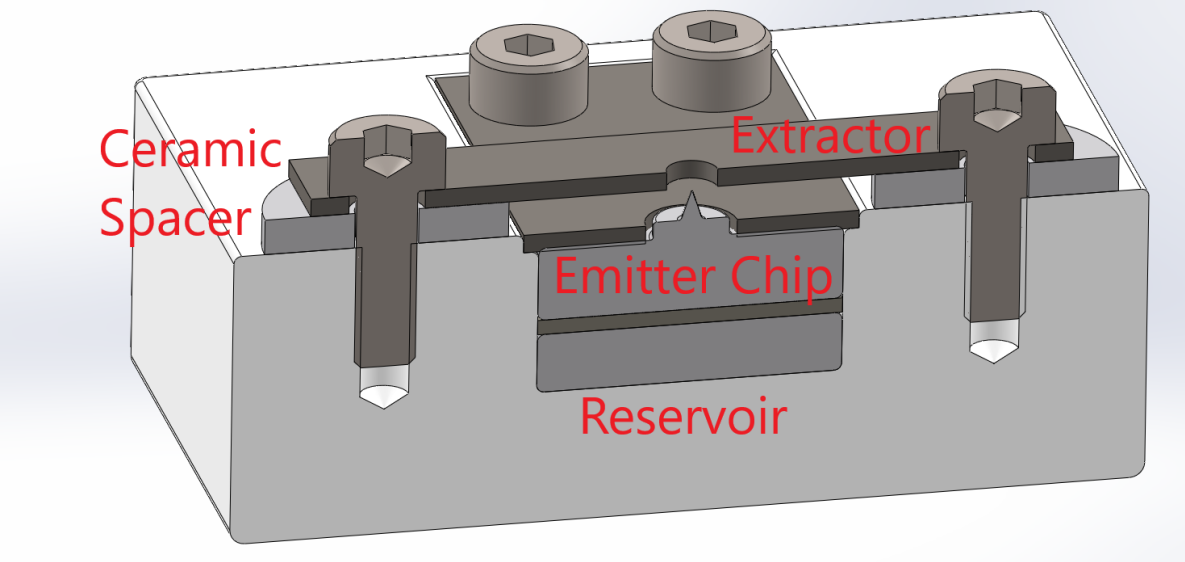

Figure 3.1: Cross section of 3D model of WeSELE.

and consistent production of the components. Second, having a single emitter enables precise characterization of emission phenomena and allows for easier diagnostic access to the emitter. As this model is acting as a baseline for future experimental campaigns, it does not include an accelerator grid. It does, however, have an easy design path to adding an accelerator grid which will enable direct comparison of thruster performance with and without an accelerator grid.

A first order estimate for the breakdown voltage for both emitter chips used in this study was calculated over a range of emitter to extractor distances using Eqs. 2.6 and 2.7. For both cases, the emitters were positioned approximately 0.5 mm from the extractor orifice. The results are plotted in Figure 3.2. The expected starting voltage is an average of the results from Eqs. 2.6 and 2.7. For EC1 the larger radius of curvature results in a higher estimated starting voltage of 1800 V, where for EC2, the starting voltage is 1300 V. The extractor grid-to-emitter tip spacing requires a balance between minimizing the starting voltage, limiting impingement of ions on the extractor plate, and decreasing beam divergence. This distance is controlled by two custom made Boron Nitride (BN) spacers.

3.2 Emitter Chip Manufacturing

The emitter chip was cut from P5 porous borosilicate glass using a lathe and diamond cutting wheel on a rotary tool. The rotary tool was mounted to the to the compound rest in place of

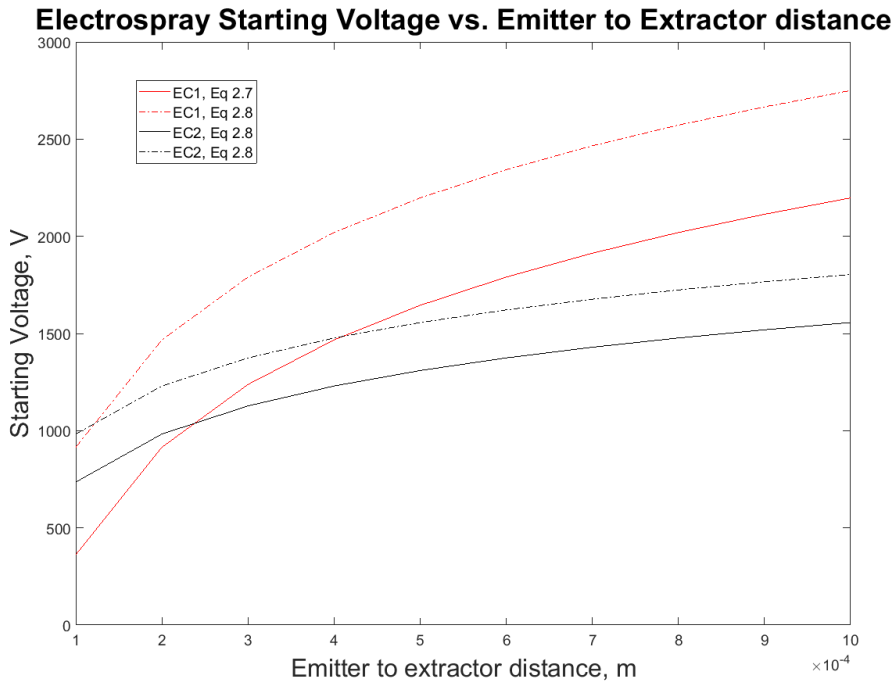

Figure 3.2: Estimated starting voltage of electrospray as a function of emitter to extractor distance.

the tool post. This enabled precise control of the cutting wheel while the work piece was turned in the chuck. Figure 3.3 shows the chip manufacturing process. Square borosilicate glass bar stock with 11.4 mm sides was mounted in a lathe with a four-jaw chuck. First, the bar stock was turned down until the 10 mm outer diameter is reached. Next, shown in Fig 3.3-B) the length for the emitter cone plus enough extra to form the platform that the emitter sits on is turned down to 2.5 mm diameter. This platform enables the entire emitter to stick out above the distal electrode. Then in 3.3- C), the rotary tool is re-positioned so the face of the cutting wheel is pressed into the glass which formed the cone. The cone is examined with a magnifier and if the tip needs to be sharpened further, diamond impregnated sandpaper is used to finish bringing the emitter to a point. DI water, which is free of contaminants that might clog pores or interact with the propellant, was constantly applied to the diamond wheel while cutting for cooling and dust suppression. Finally, the chip was parted from the bar stock and flushed with DI water then isopropyl alcohol to clear the pores of any dust from machining. Clearing the emitter chip pores using an ultrasonic bath was tested but abandoned due to it completely destroying the tips. Figure 3.4 shows a chip machined during development of this process. During storage, the emitter and reservoir are kept in a low humidity

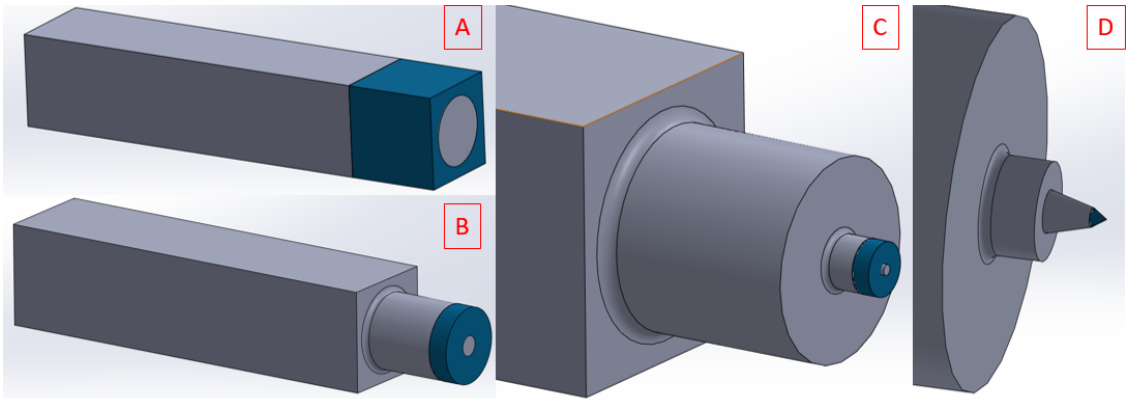

Figure 3.3: Steps for shaping porous borosilicate into single emitter cone.

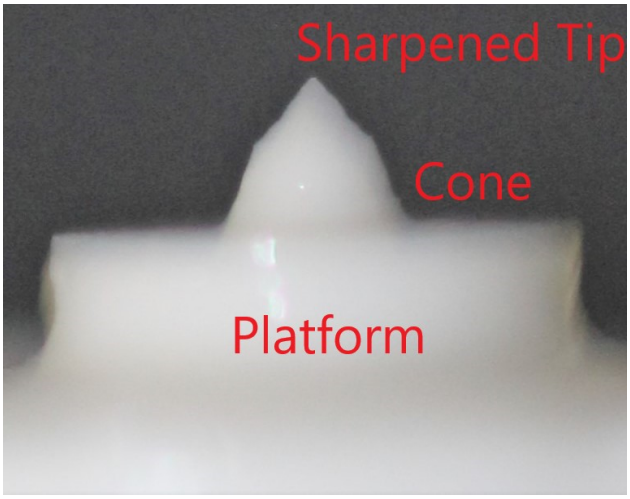

Figure 3.4: Porous borosilicate glass turned on a lathe to form a single ≈1 mm tall emitter.

and dust free environment.

All components were manufactured using the university's machine shop and ALPE's equipment. This enabled a low-cost and accessible testing platform that other universities can replicate. Solid model and CAD drawings for the emitter chip are in Appendix A. A number of different chips were manufactured during development and two with different radii of curvature were selected for use in this thesis. While this method of creating emitter chips lacks the repeatably of computer numerated control (CNC) machining it is far more accessible.

3.3 Facilities

Experiments were performed at Western Michigan University's ALPE in a 63-cm-diameter by 60-cm-long vacuum chamber equipped with a Varian MicroTorr-V 550 turbopump with a pumping speed of 550 l/s N_2 and a rotary vane backing pump. The chamber is capable of reaching a base pressure of $4.0\text{x}10^{-6}$ Torr which rises to $5.0\text{x}10^{-6}$ Torr during testing. Chamber pressure was measured using a cold cathode gauge. The emitter was biased using an EH series Glassman High Voltage Inc. power supply with output up to 10-kV and 10-mA. To obtain beam and interception current, high voltage differential probes connected to an oscilloscope measured the potential drop across sense resistors that connected the collector plate and extractor grid to ground. In-vacuum propellant loading was performed using a rotational and linear motion stage to position a syringe over the emitter and move the plunger, respectively. Greater than 98% pure EMI-BF_4 purchased from Ionic Liquid Technologies was used for all testing.

3.4 Experimental Setup

A schematic of the setup used to verify that emission was occurring and to create an I-V map of beam current and extractor grid interception current is shown in Figure 3.6. The distal electrode was biased using the Glassman power supply while the extractor grid was grounded through a 1.56 MΩ resistor. The applied voltage and current from the power supply were measured using multi-meters connected to the monitoring system on the power supply. The emitter was oriented vertically upward and centered below the turbopump in the vacuum chamber to increase the effectiveness of the pump and minimize SEE. The collector plate was positioned 12.7 mm above the extractor grid for the initial experiments and grounded through a 149.5 kΩ sense resistor. For the second round of testing a collector plate with an electron suppression grid was used and positioned 5 cm from the thruster. The in-vacuum loading system, thruster, and collector plate were all mounted on a breadboard in the vacuum chamber. Figure 3.5 shows the assembled experimental setup that was used.

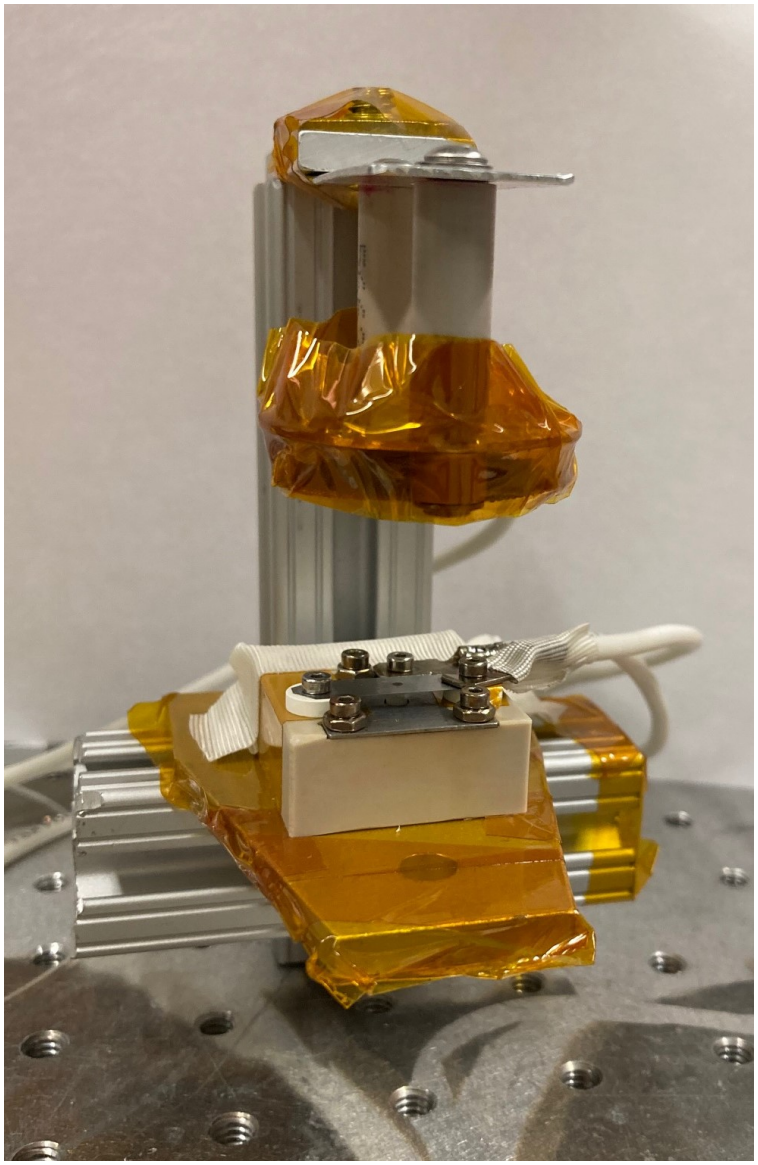

Figure 3.5: Assembled WeSELE thruster and collector plate.

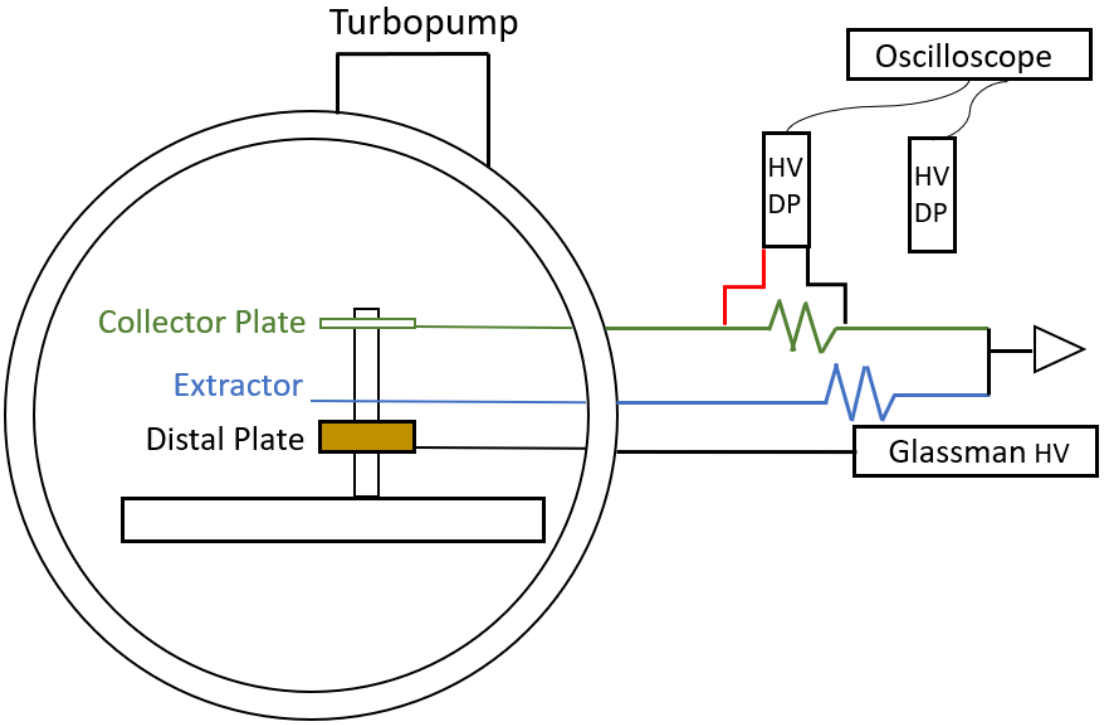

Figure 3.6: Schematic of experimental setup for testing of WeSELE.

3.5 Testing Procedure

Inconsistent operation due to gasses trapped in the porous substrate and absorbed in the propellant is detrimental to electrospray performance. To ensure steady operation a careful pre-firing process must be followed. First, the propellant was outgassed in vacuum below 1 Torr for at least 1 hour past any indication of bubble formation. The outgassed propellant is brought back up to atmospheric pressure and loaded into a syringe. The thruster and syringe are mounted in the vacuum chamber without its electrodes and outgassed for at least 24 hours at a pressure below $5.0\text{x}10^{-5}$ Torr to ensure the reservoir and emitter chip are fully evacuated. Several methods of in-vacuum loading were attempted that resulted in propellant leaking from the syringe. Bubbles were visibly expanding in the syringe, forcing the propellant out at pressures below 2 Torr. A custom in-vacuum loading system shown in Figure 3.7 was used to address this.

A rotary stage set the syringe to 90° during chamber evacuation and outgassing. This allowed the expanding gases in the syringe to escape without expelling propellant. For loading into the propellant reservoir, the rotary stage was turned so the needle was positioned over the

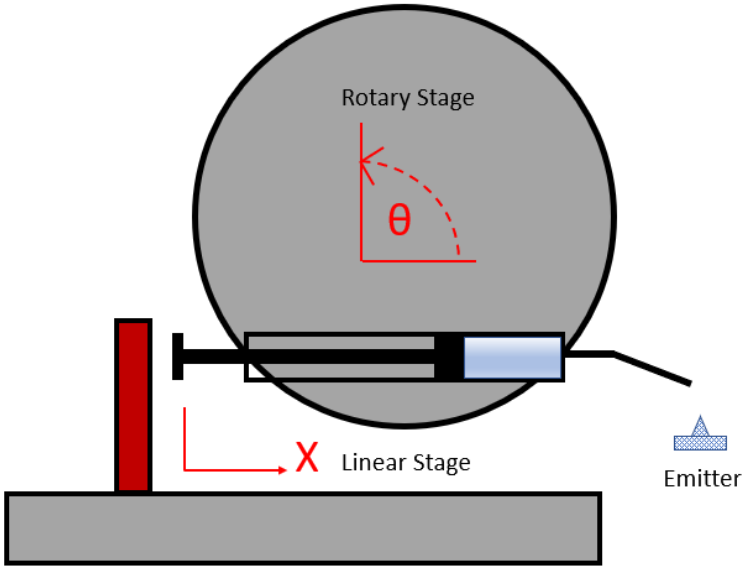

Figure 3.7: Linear and rotary stage used in combination to prevent propellant leaking from syringe during pump down.

emitter chip, and a linear stage drove the plunger along the x-axis dispensing propellant until the chip was saturated. Following this, the chamber was brought back up to atmospheric pressure, the electrodes installed, and the syringe and loading equipment removed. Results from testing that was performed without propellant outgassing or in-vacuum propellant loading showed sporadic current on the collect grid but no steady-state operation was achievable.

Once the electrodes were installed, the vacuum chamber was closed and evacuated. After the chamber reached its base pressure of $4.0\text{x}10^{-6}$ Torr with the loaded and fully assembled thruster, testing commenced. Thruster operation began by increasing voltage on the distal grid until ion emission occurred visible by current increasing above the noise floor on the collector plate. All testing was completed with the power supply operating in voltage controlled mode. Voltage was incremented in 100 V steps until thruster operation became unstable due to arcing between the distal grid and the housing bolts. Operation is validated with the concurrent rise in pressure and increase in power drawn from the supply. Time averaged collector and extractor grid current, chamber pressure, and power supply telemetry were measured and then voltage incremented.

CHAPTER 4

RESULTS AND DISCUSSION

Data were collected for three experimental setups. The first two tests successfully confirmed the emission of ions and device functionality as an electrospray thruster. All three indicators of operation were observed and are presented and discussed in the following sections. Experimentation led to the identification of several design weaknesses and improved testing practices were established that will be addressed in future work. A final round of testing showed abnormal behaviour in the interception current and collector current and will be discussed as well.

4.1 Initial Setup and Validation

For the first set of experiments, a bare aluminum sheet was used for the collector plate which results in significant secondary electron emission (SEE). However, it enabled a visual method of validating operation by observing a circular wear pattern on the plate. The wear pattern began off-center of the emitter as shown in Figure 4.1. Above an extractor to distal potential of 3000 V a second spot formed directly above the emitter. Starting the thruster above 3000 V instead of incrementally increasing voltage until 3000 V was reached still resulted in two distinct spots. This indicates a second major emission site formed on the emitter as opposed to the single emission site shifting position as voltage increased. A rise in pressure in the vacuum chamber that began at an extraction potential of 2500 V was also indicative of a mass flow from the thruster. The pressure continued to rise monotonically with voltage as shown in Figure 4.2.

4.1.1 Initial I-V Results

During initial validation of thruster operation a flawed method for measuring beam current and extractor current was implemented. Instead of using the high voltage differential probes to

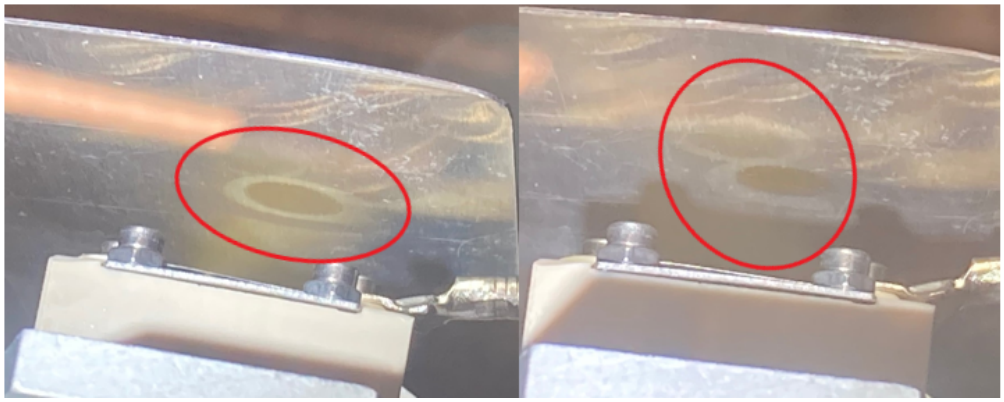

Figure 4.1: Transition of wear pattern on collector plate from single (left) to double (right) spots above 3000 V.

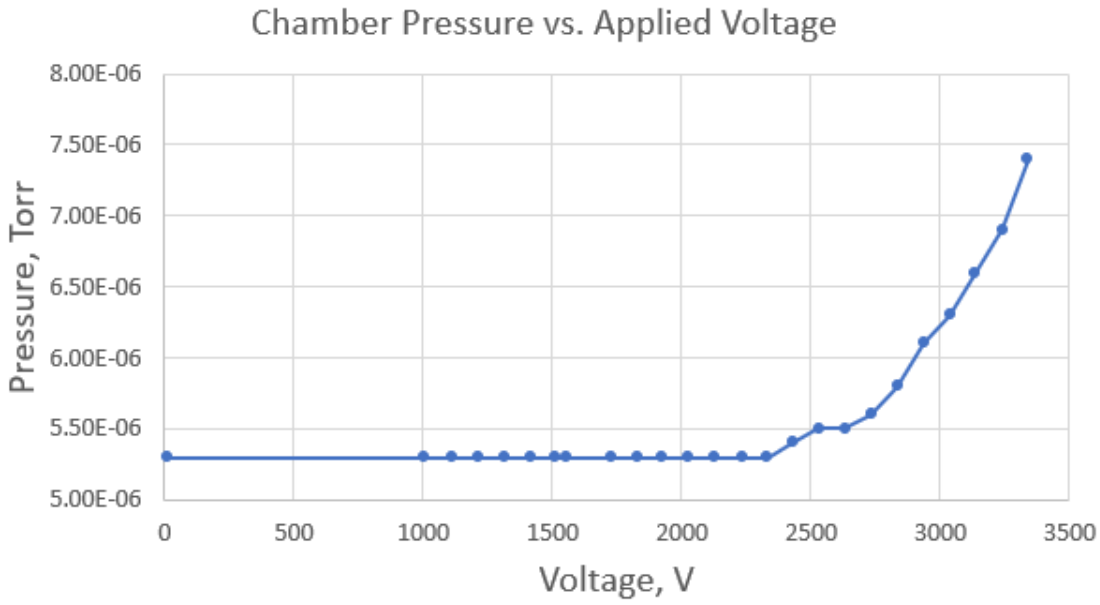

Figure 4.2: Increasing chamber pressure with increasing discharge voltage indicating emission from the electrospray.

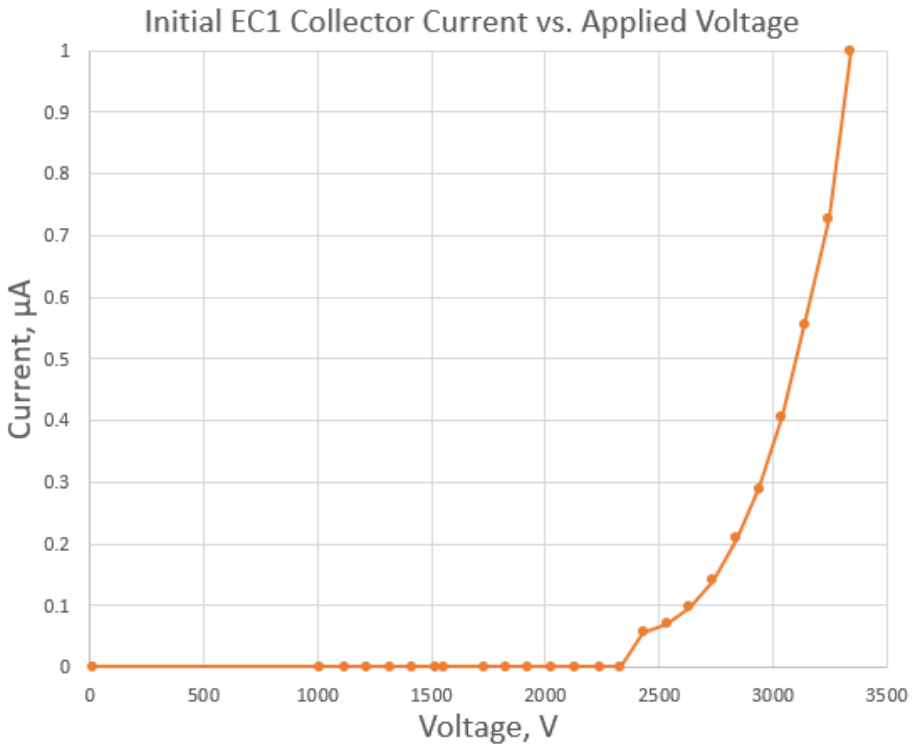

Figure 4.3: Normalized to maximum current measured on collector plate vs. applied voltage for first set of data.

measure the potential drop across resistors, the resistors were connected directly to the oscilloscope and the potential drop to ground was recorded. With the oscilloscope's inputs terminating at 1 MΩ the sense resistor for the collector current was too low to affect the voltage drop. This was shown by using a selection of resistors between 150 kΩ and 30 kΩ without significant impact on the measured voltage. While this invalidates the absolute values of the measurements, the relative trend line of nearly exponential growth of collector current with discharge voltage, which closely matches the pressure rise, proves that the thruster was operating. Figure 4.3 shows the collector plate current from this testing and Figure 4.4 shows the extractor current separately to distinguish its features.

Ion emission begins around 2400 kV, as shown in both increasing collector current and increasing background pressure. Extractor current begins rising before emission occurs due to a leak current between the distal grid and extractor grid. While collector current shows an exponential trend typical to electrosprays, the extractor current displays a more linear behavior. This is most likely a result of the leak current dominating over the current from intercepted ions. Compared to

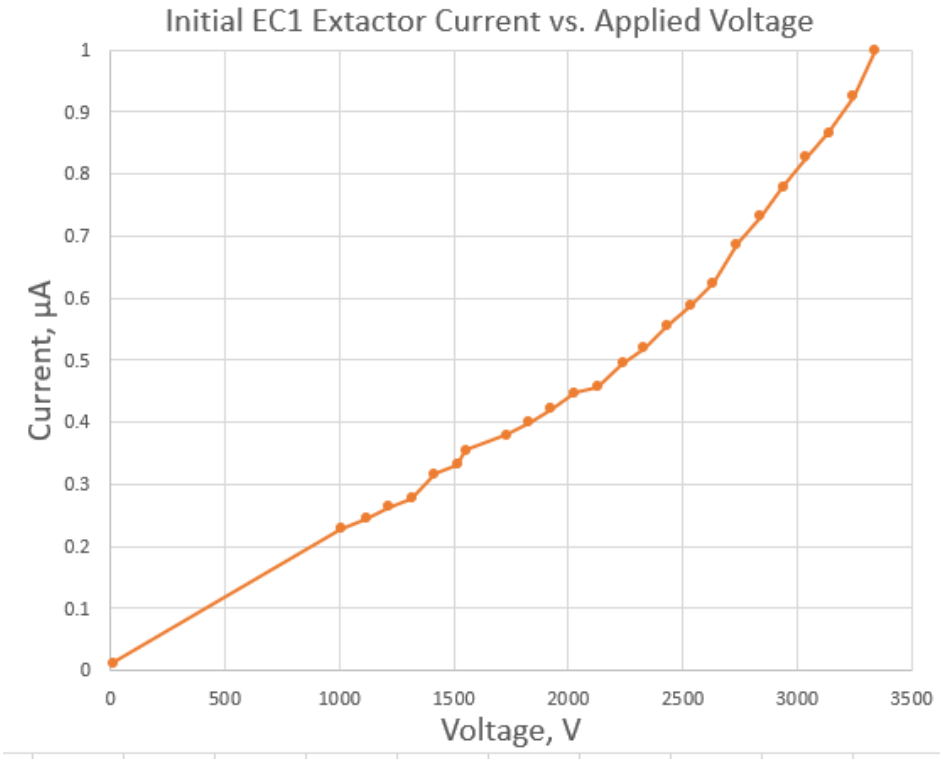

Figure 4.4: Normalized to maximum extractor current vs. applied voltage.

other ILIS that have calculated single emitter currents around 1 μA, the measured current from this data set is orders of magnitude higher. The input current from the power supply at 2800 V on the distal grid was 15μA, significantly higher than the sum of the measured currents on the collector plate and extractor grid. This clearly indicated the current measurement system to be inaccurate and had to be changed. Interestingly, the collector current data do not corroborate the existence of a second ion emission site at increased voltages. This is likely due to the inflated current values caused by the measurement method 'drowning out' the expected shift. A discontinuous jump in the emission current around 2900 V would be expected as the number of emitted ions is presumably doubled. In addition to the incorrect current measurements, a strong corona discharge was observed between the aluminum plate and thruster. The discharge can be seen in Figure 4.5 when the aluminum collector plate was mounted close to the thruster during high voltage operation. This discharge is likely due to heavy secondary electron emission from the aluminum collector plate.

Figure 4.6 shows the emitter that was used during the first experimental campaign after operation for 5 hours. Both the yellowing of the tip and the formation of solids are commonly reported in the literature but not fully understood [26] [24]. The higher starting voltage than expected

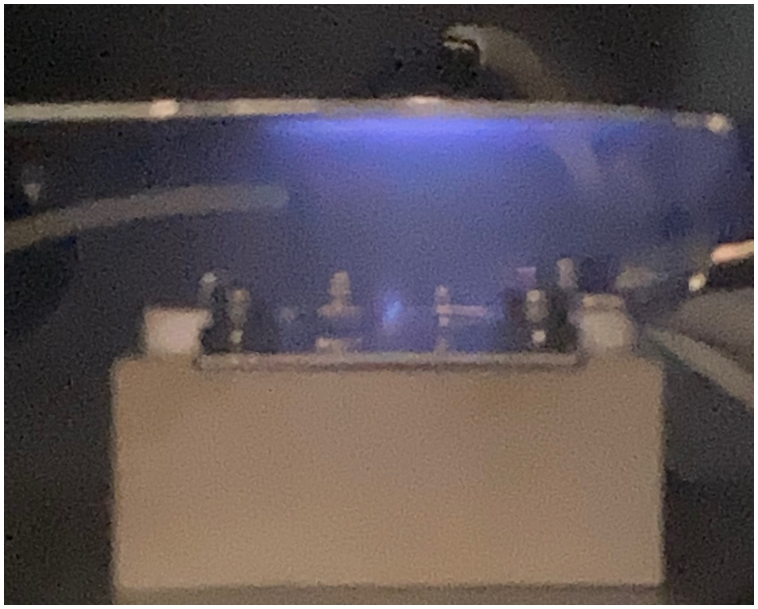

Figure 4.5: Electrospray during operation showing a plasma discharge.

based on initial calculations is attributed to the fact that emission likely did not occur at the apex of the tip and the calculated starting voltage assumed the extractor electrode did not have a orifice. The latter was indicated by the off-axis wear pattern on the aluminum collector plate. Given that offset location of the first wear pattern, it is possible the pores at the tip of the emitter were blocked and a Taylor cone formed somewhere else on the emitter, which would require a higher electric field. Additionally, extractor-to-emitter tip distance was not directly measured but calculated by the height of the emitter verses the height of the ceramic washers that supported the extractor. Some uncertainty is introduced because the extractor is not rigid and the base of the emitter is not perfectly flush with the bottom of the washers. Therefore, the actual emitter-extractor distance may not be 0.5 mm but has a margin of error of 50%.

4.1.2 Corrected I-V Results

A new method for measuring extractor and collector current was setup and the same emitter chip was flushed then refilled with propellant for a second round of testing. The sense resistor design shown in the experimental setup section of this thesis was used instead of directly terminating the resistors into the oscilloscope. The HVDP are 1 MΩ probes which match the oscilloscope terminals, eliminating the issues from the first setup. The I-V curve from 0 V to 3500 V with 100

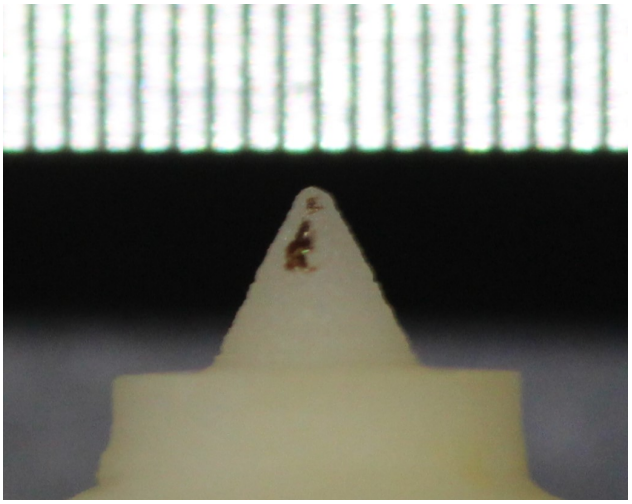

Figure 4.6: Image of the first emitter tip after operation showing yellowing and the formation of an unknown solid.

V increments above 1500 V is shown in Figure 4.7. Thruster startup occurred between 2300 V and 2400 V with the lowest emission current measured at 3.1 μA.

The results from the new system give more reasonable values with the collector current at 2800 kV being 9.1 μA and the extractor current at 0.71 μA This gives a transmission efficiency of 92%. Transmission efficiency is shown to significantly increase from 84% at 2400 V up to 96% at 3300 V. Even at 96% this is a much higher loss than what is reported in the literature of $\approx$ 99.5% by equivalent thrusters [23]. The input power at this operating point was 34 mW, and the thruster reached a maximum operating power of 280 mW at 3500 V on the distal grid.

The elevated interception of ions on the extractor grid is attributed to several factors. First, the anomalous leak current found in the initial firing is still observed in these data, albeit smaller. Second, the emitter is positioned lower below extractor than nominal resulting in some ions being directly accelerated into the extractor. Third, the inferred existence of a second emission site not at the emitter apex would significantly contribute to non-axial trajectories of ions.

Unlike in the initial tests, the I-V trace shown in Figure 4.7 of the correctly measured emission current as a function of applied extractor voltage shows a discrete jump in current around 2900 V, confirming what was observed with the second wear pattern on the collector plate. There is also a subtle but noticeable increase in the extractor current at the same potential. The second emission site being closer to the apex of the emitter may also contribute to the increasing transmission efficiency as applied voltage is increased. While the double wear pattern on the collector

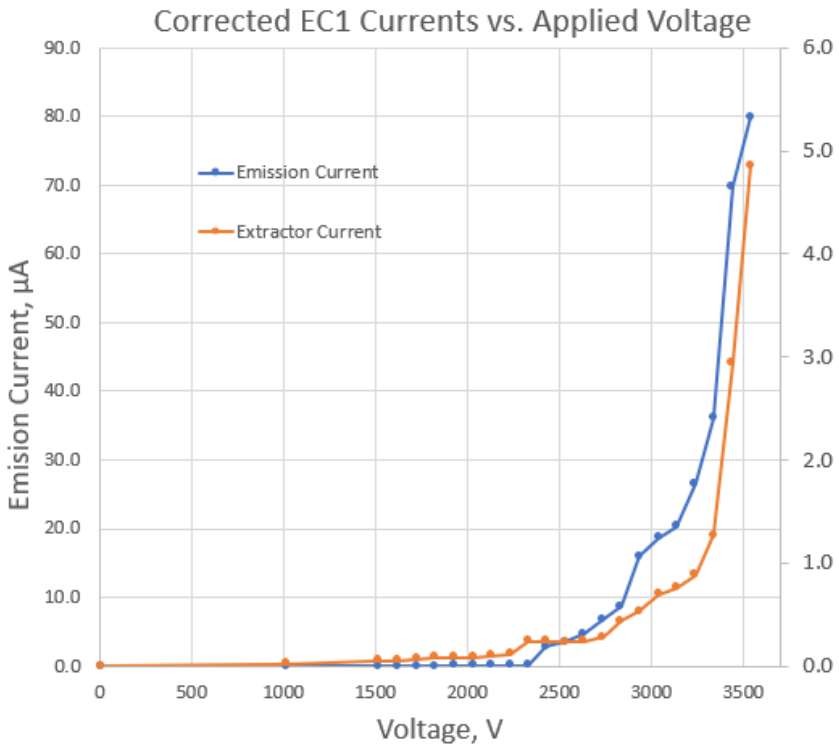

Figure 4.7: Extractor and collector current from EC1 using correct current measurement method.

plate is convincing evidence for two emission sites, validation in the telemetry is important.

The current drawn from the power supply can now be meaningfully examined with respect to the collector current. Graphing the currents against each other in Figure 4.8 shows close alignment between the two with an overall trend of the measured current being slightly lower than the input current. This is likely due to a combination of the collector plate not capturing the entire beam and an SEE current from the chamber wall. The current on the collector plate is from an anion beam therefore electrons from SEE that impact the collector plate would artificially suppress the measured current. Extractor and emission current became increasingly unstable above 3000 V as arcing occurred between the distal plate and bolts that mounted the PEEK housing to the supports. The corona discharge presumably from heavy SEE was also seen in this testing and likely affected current values.

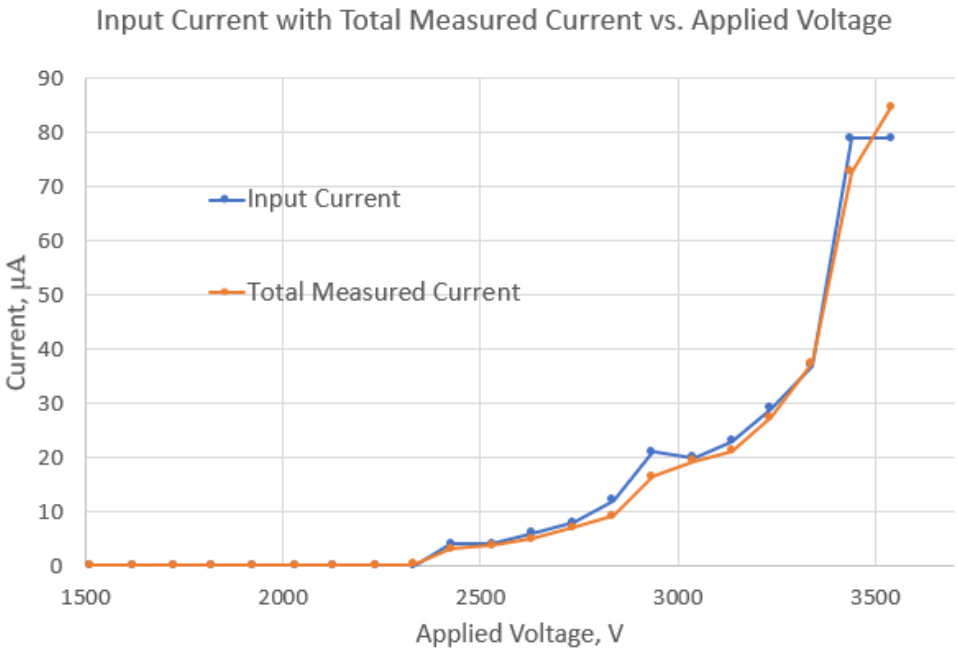

Figure 4.8: Input current measured at the power supply with sum of extractor current and emission current for EC1.

4.2 Second Emitter Chip and Enhanced Experimental Setup

A number of improvements were made to address complications that arose during the first two experiments. First, a molybdenum collector plate with an electron suppression grid replaced the aluminum collector plate. While little data exist specifically on SEE yield of metals from IL ion bombardment; molybdenum has a much lower SEE coefficient than aluminum when compared with other impinging ions. A stainless steel grid was mounted 10 mm in front of the collector plate; this grid can be negatively biased to limit SEE from the chamber walls and surrounding surfaces from reaching the collector. Additionally, the new collector plate was positioned farther away from the thruster than the first collector plate to limit the corona discharge. Second, a new emitter chip was machined with a sharper point to reduce the onset voltage and eliminate the off-center emission site. Figure 4.9 shows the new emitter tip with a smaller radius of curvature.

With the electron suppression grid in place it was not possible see wear patterns on the collector plate during operation. When the thruster was removed from the chamber after operation, discoloration on the suppression grid was observed; however, with the grid, individual wear spots

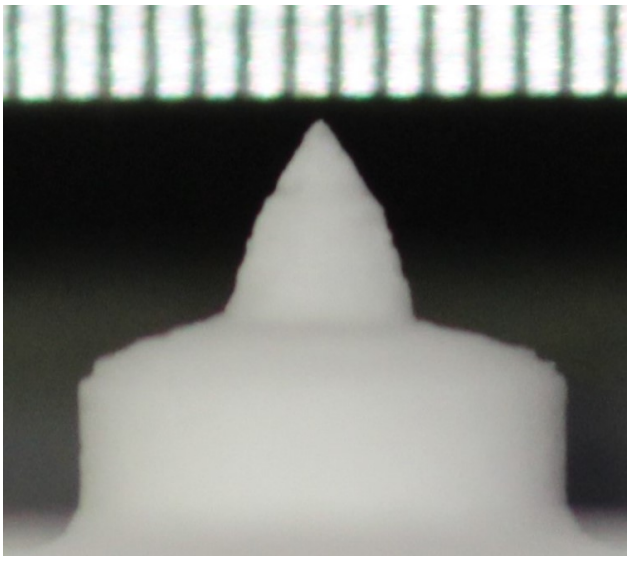

Figure 4.9: Second emitter tip used in tests before firing.

could not be distinguished. As in the first experiments, chamber pressure tracked with voltage applied to the distal electrode. These data clearly showed when propellant began being extracted from the thruster. The chamber pressure plotted in Figure 4.10 indicates emission starting at 2200 V, almost 200 V lower than with EC1. From thruster emission up to 3000 V the pressure measured during EC2 operation showed a similar trend line as what was observed with EC1. Above 3000 V the pressure began to lower and fluctuate, possibly indicating inconsistent emission.

4.2.1 EC2 I-V Results

I-V curves of extractor and emission current from EC2 operation using the new collector plate were measured from 2000 V to 2800 V in 200 V increments then 100 V increments from 2800 V to 3300 V without any potential applied to the suppression grid. These curves are shown in Figure 4.11 Current rose above the noise floor of the oscilloscope between 2000 V and 2200 V with an initial emission current of 1.54 μA and initial extractor current of 0.25 μA. Emission current maintained its exponential-like curve observed during EC1 emission, but it did not show any significant discrete changes as were observed in Figure 4.7. This indicates there was no second emission site on the smaller radius of curvature emitter. Further evidence for Taylor cone formation at the tip of the second emitter chip and no secondary emission site formation comes from comparing the magnitudes of the emission currents from EC1 and EC2. Emission current from

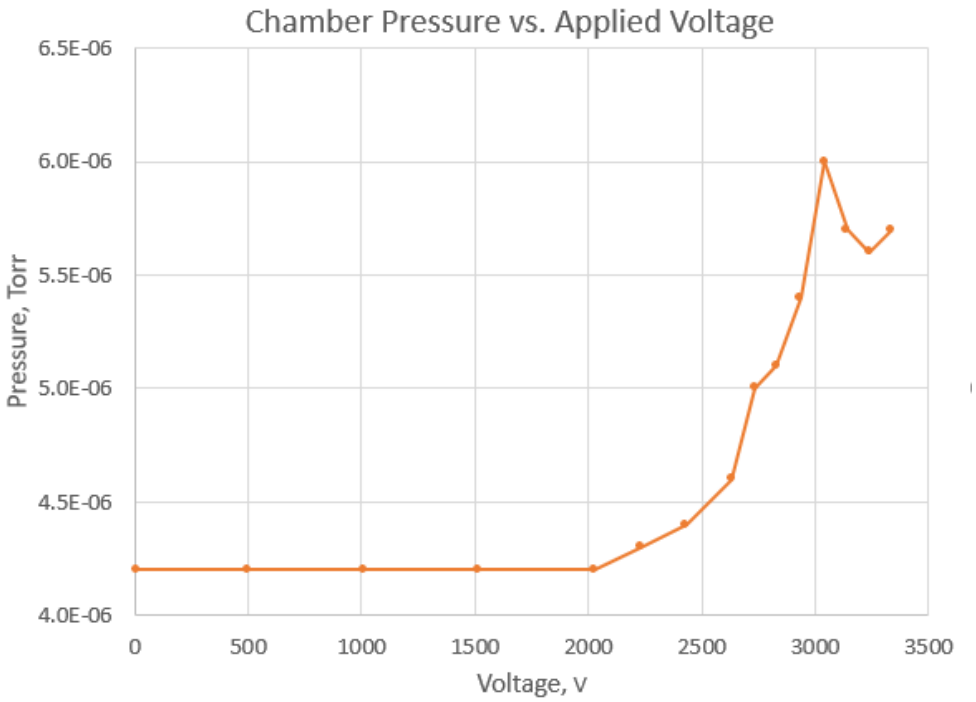

Figure 4.10: Chamber pressure as a function of applied voltage. Increase in pressure from $4.2\text{x}10^{-6}$ Torr to $4.3\text{x}10^{-6}$ Torr at 2200 V indicates first emission.

this EC2 was higher than the EC1 up to 2800 V on the distal electrode. At higher voltages, the current on EC1 jumped, surpassing that from EC2, until EC2's current growth rate brought it back above EC1.

The transmission efficiency for EC2 significantly increased with applied voltage from 84% at startup to 98.6% at 3300 V. Overall, this was higher than the transmission efficiencies measured with EC1. This, along with the lower onset voltage, is indication of emission site formation occurring at the emitter tip rather than off-center. The low initial transmission efficiency is attributed to leak current through the extractor grid as shown in Figure 4.12. Compared to extractor data from EC1, both EC2 extractor current and the anomolous current before emission (the leak current) were lower.

Next, -19 V was applied to the electron suppression grid using 9 V batteries connected in series. I-V traces of extractor and emission current were measured immediately following those measured with no voltage applied to the suppression grid to limit possible differences between the two traces. Emission occurred between 2000 V and 2200 V with an initial emission current of 2.74 μA and interception current of only 0.08 μA. This resulted in a transmission efficiency at start

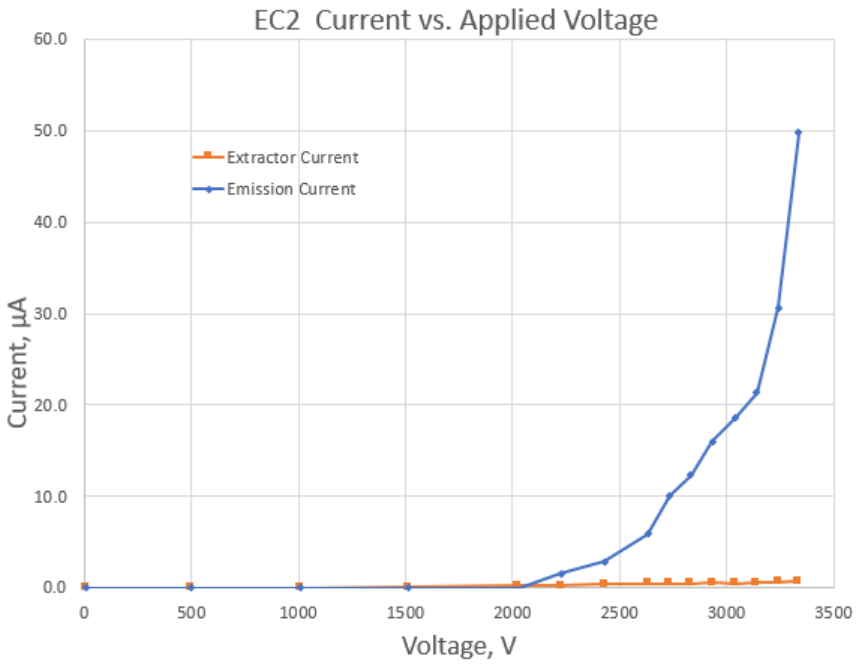

Figure 4.11: I-V curve from firing the second emitter chip without a potential applied to the suppression grid.

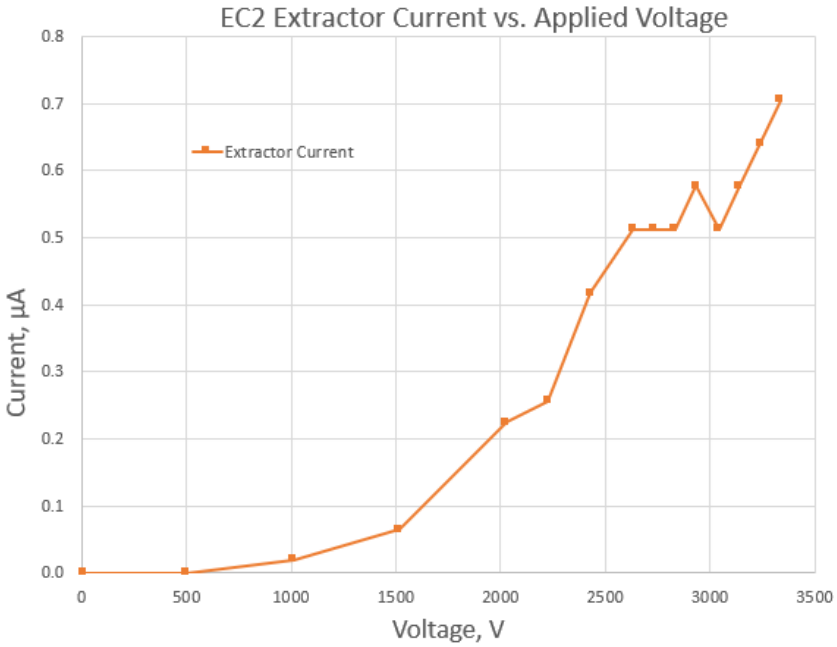

Figure 4.12: Extractor current from firing EC2. Note, current is measured before emission begins at 2200 volts.

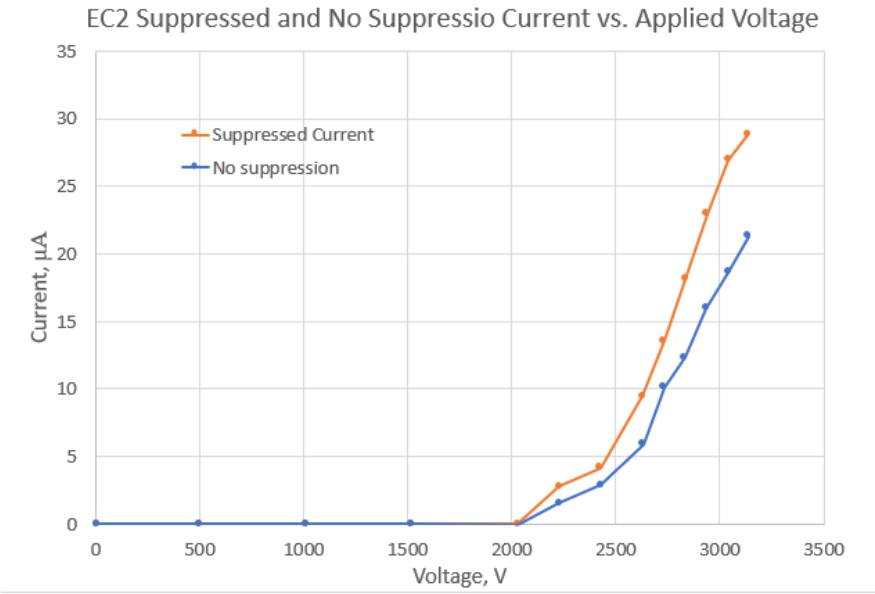

Figure 4.13: Comparison of emission current with suppression grid voltage set to -19 V and 0 V.

up of 97%. The data from this operation shows transmission efficiencies between 96% and 99%. Without plume data it is not possible to calculate the beam power; however, a peak input power of 97 mW was calculated for the 3100 V operating condition. The increased transmission is not only a result of the increased emission current from rejecting SEE electrons. Unexpectedly, the interception current was lower during the SEE experiment compared to the previous experiment with no suppression grid potential even though no changes were made to the thruster. It is possible that sufficient time was not allowed for extractor currents to settle to their actual values between measurements during the initial EC2 experiment, resulting in artificially high results from the first IV trace. Figure 4.13 shows the current on the collector plate for both experiments with EC2. The current for the case with SEE suppression is higher at equivalent applied voltages than what is observed without SEE suppression. Results from EC2 with applied electron suppression potential represent the most accurate emission current data from the experimental campaign. Additionally, the corona discharge was not visible for data measured using the new molybdenum collector plate positioned farther from the thruster.

Comparing the input current to the total measured current in Figure 4.14 from firing the thruster with the suppression grid shows the input current to still be slightly higher than the sum of the measured currents. It is likely the new collector plate is also not capturing the full beam.

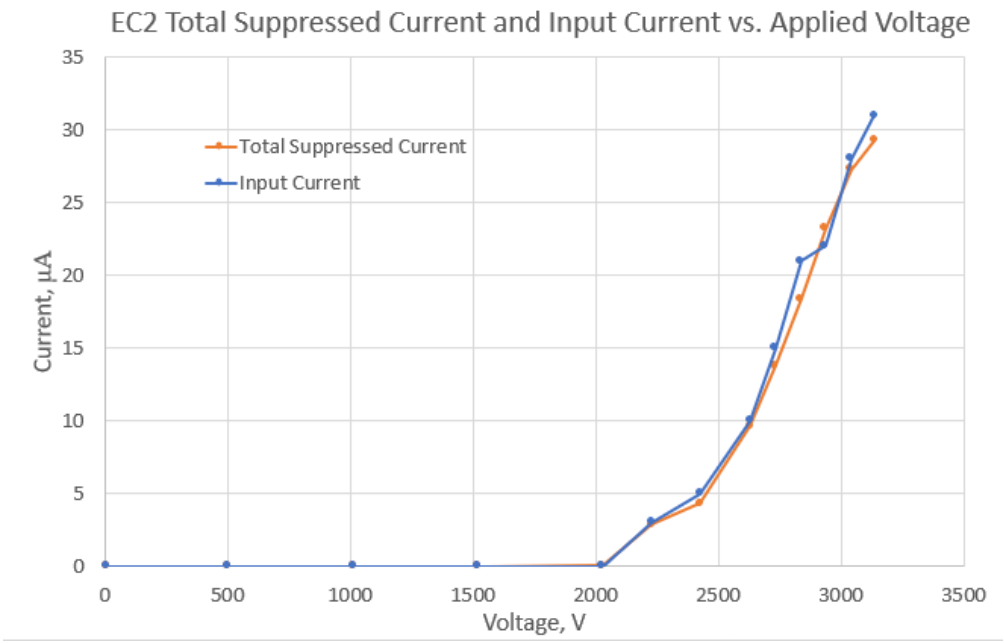

Figure 4.14: Sum of emission and extractor current plotted with input current when suppression grid potential is at -19 plotted against applied distal voltage.

Additionally, only one suppression potential was tested and electrons from the surroundings may still have made it to the collector. SEE on the collector plate itself is most likely also occurring. This would mean, because the SEE yield from aluminum is greater than molybdenum the actual difference between input current and total measured current from the first experimental setup would be smaller than shown. Therefore, a greater portion of the error from the first setup was correcting the error from surroundings SEE and not entirely capturing the plume; where as the new collector plate had less SEE making these same errors more prevalent.

4.3 Experimental Challenges

The experimental setup using EC2 successfully addressed many of the issues with the first setup; however, several problems were still encountered. When stepping up the applied voltage to the extractor grid at potentials above 2800 V, the interception and emission currents would spike then settle after a few seconds. Above a 3000 V potential difference between the propellant and the extractor grid, significant arcing occurred, resulting in a maximum voltage of 3100 V for EC2 instead of the previous 3500 V for EC1. Figure 4.15 shows the burn marks between where the

Figure 4.15: Image of WeSELE after operation with distal and extractor grid removed.

distal grid was and the housing bolts from arcing on the electrospray thruster after firing. Figure 4.15 also shows a single spot of discoloration on the emitter chip where contact between the distal grid and emitter chip is made. This indicates a poor electrical connection to the propellant which could affect performance.

An AC component of the emission current was also captured with the oscilloscope around extraction voltages of 3000 V. A sinusoidal signal would manifest for several seconds before the system returned to a purely DC signal with no other changes in operation. Examples of the oscillations are shown in appendix B. Another challenge for the work performed in this thesis was that all data in were collected manually instead of with a DAQ. This introduces unnecessary human error into the results compared to measurements made programmatically.

CHAPTER 5

CONCLUSION

A single emitter porous borosilicate ionic liquid ion source was successfully developed and tested. Emission current and interception current from two emitter chips were measured as a function of applied voltage between the distal electrode and the extractor grid at voltages varying from 0 V to 3500 V. The affect of electron suppression on measured emission current was also tested. Through these measurements, WeSELE was demonstrated to be an effective test platform for future electrospray research. A number of key challenges and areas for improvement for the thruster have been identified throughout testing.

5.1 Concluding Remarks

The Western Single Emitter Laboratory Electrospray (WeSELE) was designed, and thruster operation was validated by visual observations, telemetry and beam current measurements. During the design process a method for fabricating a single porous borosilicate emitter on a lathe was developed and two resulting emitter chips were selected for testing. An in-vacuum loading process for EMI-BF_4 was also developed and used to ensure steady thruster operation. Two sets of experiments were performed: (1) an initial validation of thruster function using an EC1 with an $\approx$0.1 mm radius of curvature and a bare aluminum plate as a beam dump, (2) characterisation of performance of EC2 with an $\approx$0.03 mm radius emitter with a molybdenum beam dump covered by an electron suppression grid and (3) demonstration of SEE suppression using the suppression grid at -19 V. Background chamber pressure, input current at the extractor power supply, voltage between the distal plate and the extractor grid, current on the collector plate, and current on the extractor grid were measured for varying applied voltages. Interception and emission current were measured using high-voltage differential probes across sense resistors, tying the respective

electrodes to ground.

Results from the EC1 showed emission current starting at 3.1 μA at 2400 V and reaching 80 μA at 3500 V. Observation of two distinct wear marks on the collector plate along with a corresponding jump in emission current around 3000 V points to the formation of a second emission site. A leak current through the extractor grid resulted in a low transmission efficiency of 84% at startup which increased to 96% at 3500 V. The low efficiency may also be due to the first emission site not being at the apex of the emitter tip. This is inferred by the off-center wear pattern on the collector plate. Additionally, this off-center emission may have contributed to the high onset voltage. A strong corona discharge observed during testing along with knowledge of SEE from aluminum prompted the replacement of the aluminum collector plate. A new emitter tip, EC2, with smaller radius of curvature was also made to decrease onset voltage and eliminate the secondary emission site.

I-V curves of from EC2 telemetry data were produced for voltages ranging from 0 V to 3300 V using the new electron suppression grid and collector plate. Emission started between 2000 V and 2200 V at 1.54 μA on the collector plate without biasing the suppression grid. Extractor current started at 0.25 μA and increased to 0.71 μA at 3300 V a marked decrease compared to interception current for EC1. Emission current reached 50 μA at 3300 V resulting in the transmission increasing from 84% to 98.6% over the voltage sweep. I-V curves with the electron suppression grid set to -19 V were measured immediately following the initial EC2 tests without suppression grid voltage. Emission current was significantly higher at all applied voltages, indicating SEE from the surrounding chamber and hardware contributed a large current. No corona discharge was observed using the new experimental setup implying the results are closer to reality. Arcing occurring at extractor grid voltages above 3000 V remained a limiting factor in this experimental setup.

5.2 Future Work

As stated in the introduction the thruster developed in this thesis is intended to open a new avenue of research for ALPE. Therefore, a large portion of the proposed future work will be actual experimental campaigns investigating electrospray operating phenomena. The thruster was

designed with a single emitter so that fundamental processes could be characterized without performance artifacts from arrayed operation obscuring results. The overall geometry of the thruster is also intended to be robust and easily modifiable. Preceding any new experimental campaigns, a number of updates to the thruster and experimental setup should be made along with a more thorough characterization of performance.

First, the other half of I-V curves from 0 V to -3500 V should be obtained. ALPE has recently obtained a Stanford Research Systems bipolar power supply that can perform this characterization. It will also benefit future research to characterize the plume with an RPA and a FP. These will allow for the calculation of beam voltage and plume divergence angle, respectively. A series of long-duration firings at constant operating conditions should also be completed. By massing the thruster before and after each test an estimate of the mass flow rate of the thruster can be calculated as a function of throttle point. Additionally, a new emitter chip will be manufactured and dry fired without propellant to better identify were the extractor leak current observed in testing originates. A new design of the PEEK housing will be made to address arcing based on the EC2 experiments that showed the mounting bolts to be a source. Finally, a new method for positioning the extractor plate will be included in this housing redesign that will enable easier assembly and quick adjustment of emitter to extractor distance.

For the experimental setup a larger collector plate that can fully capture the exhaust plume should be made. A rigorous study of electron suppression bias should also be completed to identify the best potential for repelling SEE electrons without affecting the plume. Along with this a Labview VI and DAQ system for collecting telemetry data will significantly enhance the operating procedure and provide more accurate results. Additionally, the ability to switch discharge polarity at 1 Hz will be implemented.

Several possible studies have already been proposed utilizing this new platform. Mass flow rate is an important parameter in propulsion for characterizing thruster performance. The passive feed system for ILIS makes it difficult to directly obtain mass flow rate. The current state-of-the-art method is to mass the thruster in-vacuum before and after several minutes or even hours of operation. ALPE has designed a new system for in-situ, real-time mass flow rate measurements that could be implemented on flight thrusters. Lifetime and thrust efficiency are both heavily driven by ion dynamics at the emitter tip. A method for directly imaging ion emission for the first time

at the emitter tip using laser-induced fluorescence has also been developed. Pending funding, this study will be carried out on a modified version of WeSELE for better optical access to the emitter.

REFERENCES

[1] Stephanie DelPozzo, Caleb Williams, and Bill Doncaster. 2019, NANO / MICROSATELLITE Market Forcast. Technical report, SpaceWorks Enterprises, Inc, Atlanta, 2019.

[2] Kristina Lemmer. Propulsion for CubeSats. *Acta Astronautica*, 134(January):231–243, 2017.

[3] Igor Levchenko, Kateryna Bazaka, Yongjie Ding, Yevgeny Raitses, Stéphane Mazouffre, Torsten Henning, Peter J. Klar, Shunjiro Shinohara, Jochen Schein, Laurent Garrigues, Minkwan Kim, Dan Lev, Francesco Taccogna, Rod W. Boswell, Christine Charles, Hiroyuki Koizumi, Yan Shen, Carsten Scharlemann, Michael Keidar, and Shuyan Xu. Space micropropulsion systems for Cubesats and small satellites: From proximate targets to furthermost frontiers. *Applied Physics Reviews*, 5(1):36, 2018.

[4] Michael Keidar, Taisen Zhuang, Alexey Shashurin, George Teel, Dereck Chiu, Joseph Lukas, Samudra Haque, and Lubos Brieda. Electric propulsion for small satellites. *Plasma Physics and Controlled Fusion*, 57(1), 2015.

[5] Paulo C. Lozano, Brian L. Wardle, Padraig Moloney, and Suraj Rawal. Nanoengineered thrusters for the next giant leap in space exploration. *MRS Bulletin*, 40(10):842–849, 2015.

[6] Dan M. Goebel and Ira Katz. *Fundamentals of Electric Propulsion: Ion and Hall Thrusters*. Wiley, 1st edition, 2008.

[7] Dan R. Lev, Roger M Myers, Kristina M Lemmer, Jonathan Kolbeck, Michael Keidar, Hiroyuki Koizumi, Daren Yu, Tony Schoenherr, Jose Gonzalez, Wonho Choe, Riccardo Albertoni, W. Andrew Hoskins, Shen Yan, William Hart, Richard Robert Hofer, Ikkoh Funaki, Alexander Lovtsov, Kurt A. Polzin, Anton Olshaskii, and Olivier B. Duchemin. The Technological and Commercial Expansion of Electric Propulsion in the Past 24 Years. In *35th IEPC*, number October, pages IEPC–2017–242, Atlanta, Georgia, 2017.

[8] Rodney L. Burton. Pulsed Plasma Thrusters. *Encyclopedia of Aerospace Engineering*, pages 1–12, 2010.

[9] Michael Tsay, Kurt Hohman, and Lynn Olson. Micro RF Ion Engine for Small Satellite Applications. *23rd Annual AIAA/USU Conference on Small Satellites*, pages 1–6, 2009.

[10] Shibdas Banerjee and Shyamalava Mazumdar. Electrospray Ionization Mass Spectrometry: A Technique to Access the Information beyond the Molecular Weight of the Analyte. *International Journal of Analytical Chemistry*, 2012:1–40, 2012.

[11] John K Ziemer, Colleen M Marrese-reading, Steven M Arestie, David G Conroy, Stephanie D Leifer, and Alejandro Lopez Ortega. Incorporating Lessons Learned into LISA Colloid Microthruster Technology Development. In *AIAA Propulsion and Energy Forum*, number August, pages 1–15, Indianapolis, 2019. AIAA.

[12] Bertrand Mennesson. HabEx: Habitable Exoplanet Observatory Final Report. Technical report, Jet Propulsion Laboratory, Pasadena, CA, 2019.

[13] Anirudh Thuppul, Peter L. Wright, and Richard E. Wirz. Lifetime considerations and estimation for electrospray thrusters. *2018 Joint Propulsion Conference*, pages 1–12, 2018.

[14] Peter L Wright, Henry Huh, and Mckenna J Davis. Assessment of Grid Impingement for Electrospray Thruster Lifetime. (September):1–18, 2019.

[15] Geoffrey Taylor. Disintegration of water drops in an electric field Sir Geoffrey Taylor. (February), 1964.

[16] B. J. Wild, B. N. Green, E. K. Cooper, M. R.A. Lalloz, S. Erten, A. D. Stephens, and D. M. Layton. Rapid identification of hemoglobin variants by electrospray ionization mass spectrometry. *Blood Cells, Molecules, and Diseases*, 27(3):691–704, 2001.

[17] Anthony D. Duong, Gang Ruan, Kalpesh Mahajan, Jessica O. Winter, and Barbara E. Wyslouzil. Scalable, semicontinuous production of micelles encapsulating nanoparticles via electrospray. *Langmuir*, 30(14):3939–3948, 2014.

[18] M. N. Huberman, J. C. Beynon, E. Cohen, D. S. Goldin, P. W. Kidd, and S. Zafran. Present status of colloid microthruster technology. *Journal of Spacecraft and Rockets*, 5(11):1319–1324, 1968.

[19] I. Romero-Sanz, R. Bocanegra, J. Fernandez de la Mora, and M. Gamero-Castaño. Source of heavy molecular ions based on Taylor cones of ionic liquids operating in the pure ion evaporation regime. *Journal of Applied Physics*, 94(5):3599–3605, 2003.

[20] Richard E. Wirz, Adam L. Collins, Anirudh Thuppul, Peter L. Wright, Nolan M. Uchizono, Henry Huh, Mckenna J. Davis, Johnathan K. Ziemer, and Nathaniel R. Demmons. Electrospray Thruster Performance and Lifetime Investigation for the LISA Mission. *AIAA Propulsion and Energy*, (August), 2019.

[21] David Krejci, Valentin Hugonnaud, Tony Schönherr, Bryan Little, Alexander Reissner, Quirin Koch, Eduard Bosch Borràs, and José González Del Amo. Full Performance Mapping of the IFM Nano Thruster including Direct Thrust Measurements. *Journal of Small Satellites*, 8(2):881–893, 2019.

[22] David Krejci, Fernando Mier-Hicks, Corey Fucetola, Paulo Lozano, Andrea Hsu Schouten, and Francois Martel. Design and Characterization of a Scalable ion Electrospray Propulsion System. *Joint Conference of 30th ISTS, 34th IEPC and 6th NSAT, Hyogo-Kobe, Japan*, pages 1–11, 2015.

[23] Michael R. Natisin and Henry L. Zamora. Performance of a Fully Conventionally Machined Liquid-Ion Electrospray Thruster Operated in PIR. In *International Electric Propulsion Conference 2019*, pages 1–16, Vienna, Austria, 2019.

[24] Robert J Antypas and Joseph J Wang. Pure Ionic Electrospray Extractor Design Optimization. pages 1–9, 2019.

[25] Chase S. Coffman and Paulo C. Lozano. On the Manufacturing and Emission Characteristics of Dielectric Electrospray Sources. pages 1–12, 2013.

[26] David Krejci, Fernando Mier-Hicks, Robert Thomas, Thomas Haag, and Paulo Lozano. Emission characteristics of passively fed electrospray microthrusters with propellant reservoirs. *Journal of Spacecraft and Rockets*, 54(2):447–458, 2017.

[27] Chengjin Huang, Jianling Li, and Wei Fan. The Current Analysis of Electrospray Process on a Single Emitter with Ionic Liquid for Micro Propulsion. pages 1–15, 2020.

[28] B. Gassend, L. F. Velásquez-García, A. I. Akinwande, and M. Martínez-Sánchez. A fully integrated microfabricated externally wetted electrospray thruster. *Collection of Technical Papers - 43rd AIAA/ASME/SAE/ASEE Joint Propulsion Conference*, 2:1731–1738, 2007.

[29] Daniel Courtney, Hanqing Li, Paulo Lozano, PabloDiaz GomezMaqueo, and Timothy Fedkiw. On the Validation of Porous Nickel as Substrate Material for Electrospray Ion Propulsion. (July), 2010.

[30] Natalya Brikner and Paulo C. Lozano. The role of upstream distal electrodes in mitigating electrochemical degradation of ionic liquid ion sources. *Applied Physics Letters*, 101(19), 2012.

[31] Daniel G. Courtney and Herbert Shea. Influences of porous reservoir Laplace pressure on emissions from passively fed ionic liquid electrospray sources. *Applied Physics Letters*, 107(10), 2015.

[32] Alyssa M Ralph, Andrea G Hsu, Jason A Young, and Thomas J Curtiss. Characterization of a Single Emitter Electrospray Thruster. Technical report, Space and Missile Systems Center, El Segundo, 2016.

[33] Trevor Morris, Cecile Malardier-jugroot, and Manish Jugroot. Characterization of electrospray beams for micro-spacecraft electric propulsion applications. *Journal of Electrostatics*, 71(5):931–938, 2013.

[34] MIT OpenCourseWare. Session 20: Electrospray Thrusters, 2015.

[35] Daniel L Brown, Mitchell L R Walker, James Szabo, Wensheng Huang, and John E Foster. Recommended Practice for Use of Faraday Probes in Electric Propulsion Testing. *JOURNAL OF PROPULSION AND POWER*, 33(3):582–613, 2017.

[36] Robert B Lobbia and Brian E Beal. Recommended Practice for Use of Langmuir Probes in Electric Propulsion Testing. *JOURNAL OF PROPULSION AND POWER*, 33(3):566–581, 2016.

[37] Bolton Ferda. Retarding Potential Analyzer Theory and Design. Technical report, Princeton University, 2015.

APPENDIX A

Thruster Drawings and 3D Model

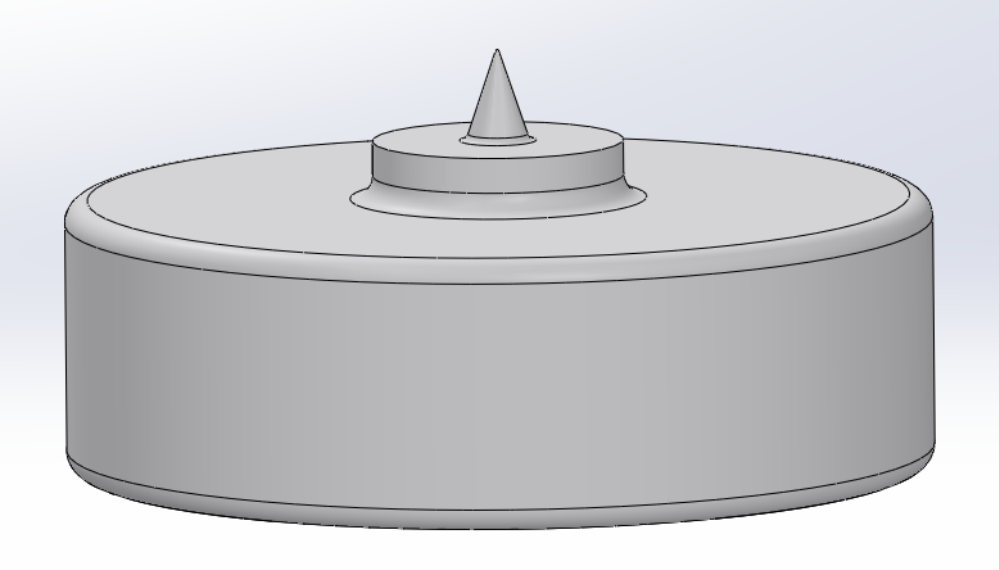

Figure A.1: 3D SolidWorks model that was used in the design and planning of WeSELE.

Engineering drawings and a solid model of the emitter chip along with an exploded view of the entire thruster are presented here. Exact dimensions of the apex of the emitter chips varied because tip formation was finished by hand using diamond sandpaper.

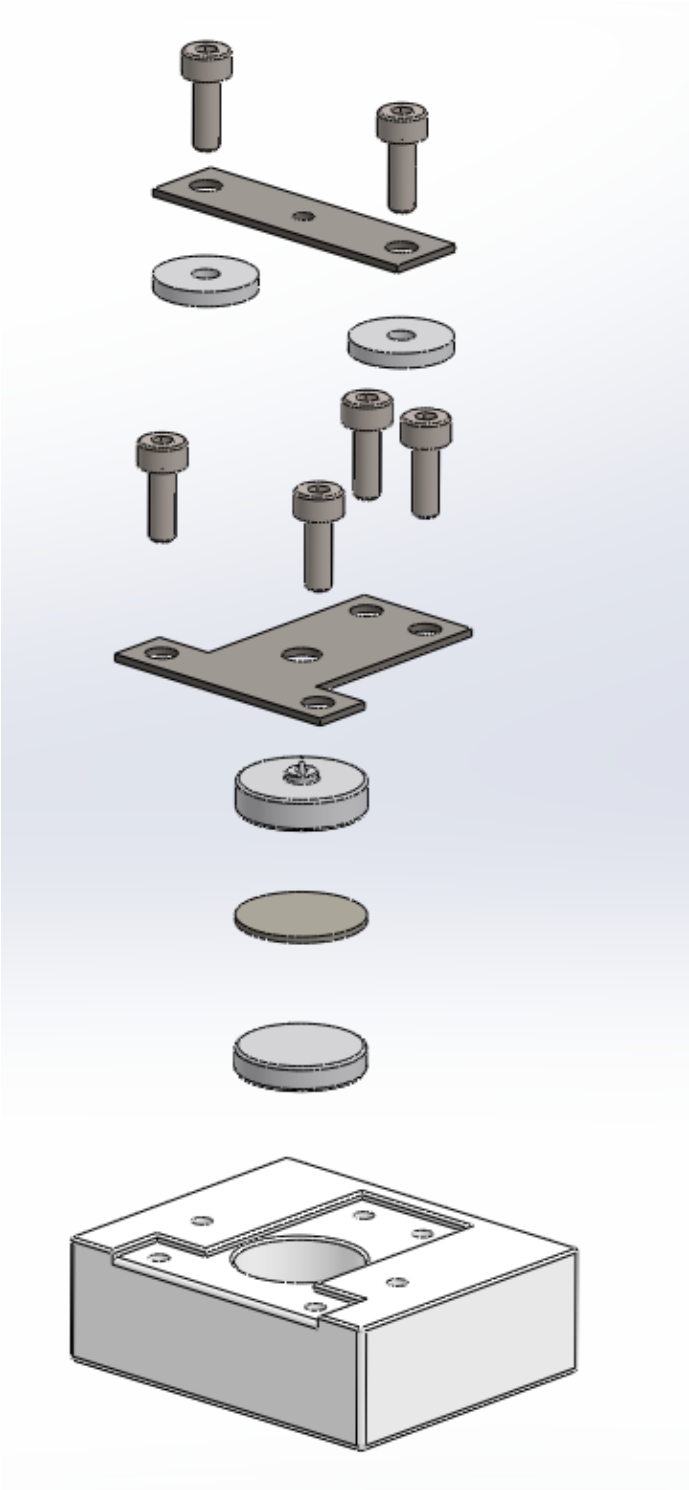

Figure A.2: Exploded view of the 3D model designed in SolidWorks for the WeSELE.

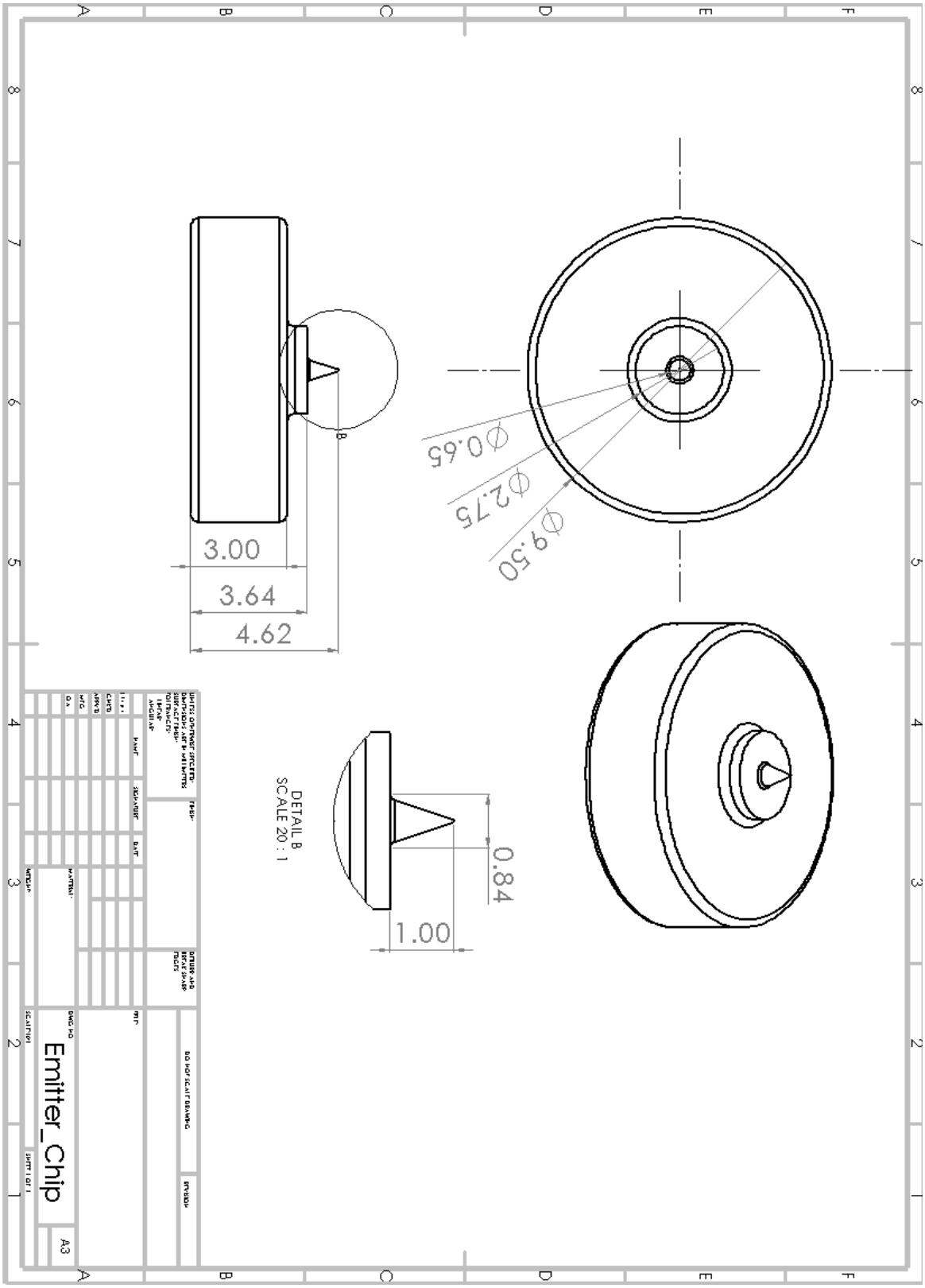

Figure A.3: Dimensioned engineering drawing in mm = millimeters used during the fabrication of the porous borosilicate emitter chip.

APPENDIX B

Oscillations in Emission Current

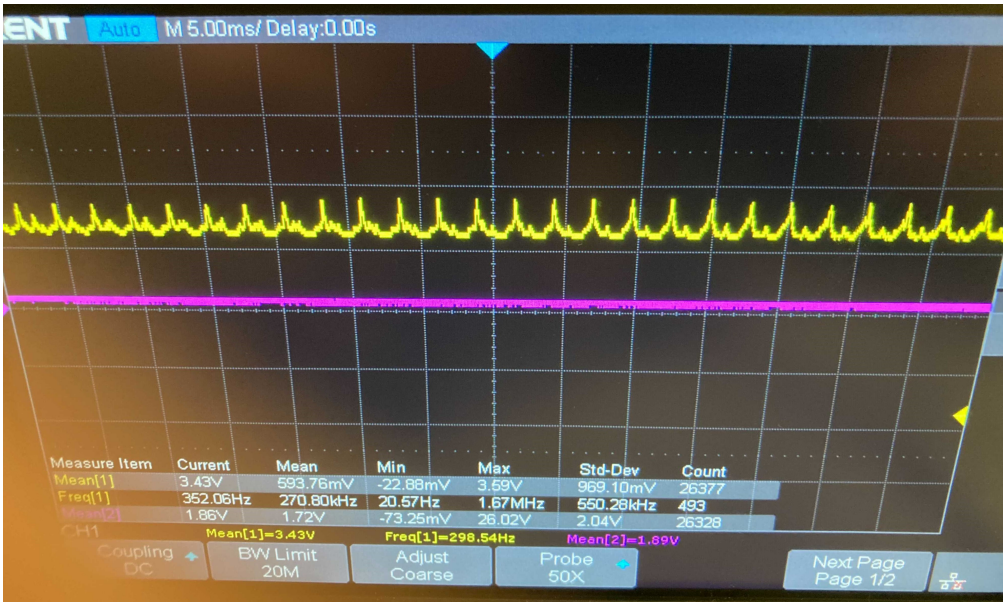

Figure B.4: Picture of the oscilloscope display while oscillation was present.

Above 3000 V oscillations in the emission current would be periodically seen. This AC component of the emission current would manifest for 30-60 second then return to steady-state. Figure 1-3 show examples of this phenomena. No explanation of this occurrence is immediately obvious and further investigation is needed. The frequency, amplitude, and shape changed between occurrences sometimes manifesting as a saw-tooth pattern or close to a sinusoid.

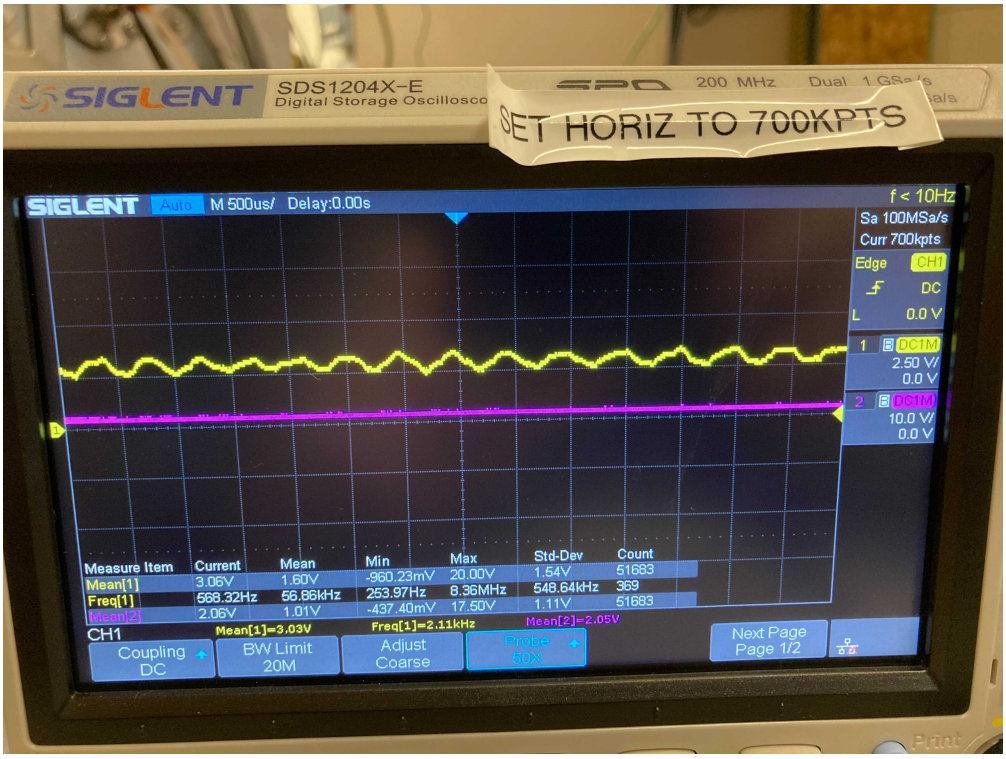

Figure B.5: A different mode of this oscillation with a more sinusoidal appearance.

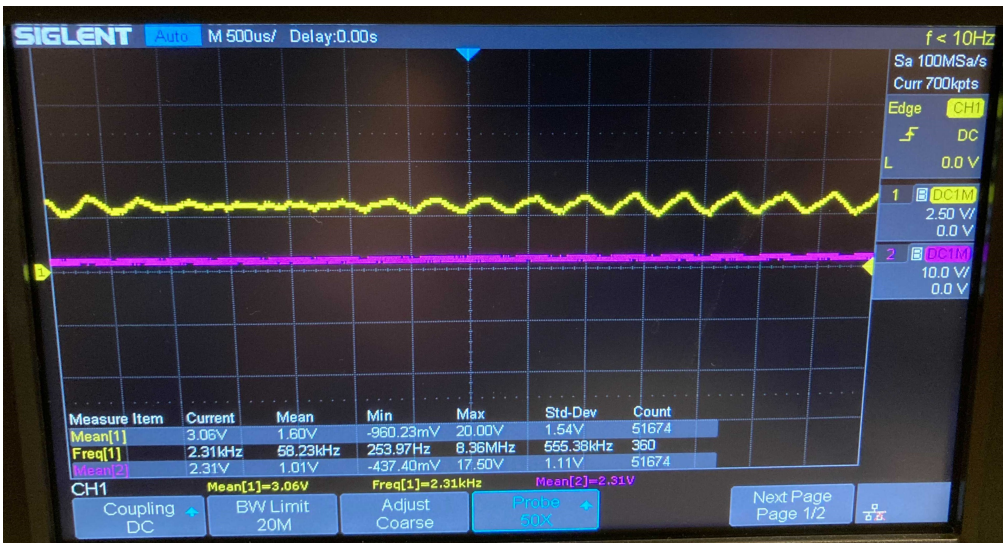

Figure B.6: A third example with different amplitude and frequency.